Applied Mathematical Modelling 139 (2025) 115812

Contents lists available at ScienceDirect

Applied Mathematical Modelling

journal homepage: www.elsevier.com/locate/apm

Exact H_∞ optimization of dynamic vibration absorbers: Univariate-polynomial-based algorithm and operability analysis

Yifan Liu, Li Cheng *

Department of Mechanical Engineering, The Hong Kong Polytechnic University, Kowloon, Hong Kong, China

ARTICLE INFO

Keywords:
Dynamic vibration absorber
Exact H_∞ optimization
Optimization framework
Operability analysis

ABSTRACT

H_∞ optimization of dynamic vibration absorbers (DVAs) to minimize the maximum response amplitude of primary structures is a classical topic. The commonly used fixed-point method only provides approximate solutions requiring the primary structure is undamped. Instead, we perform exact optimization and investigate the less-reported parametric effects on optimization operability. To handle the known restrictions posed by grounded dampers, a typical DVA model mounted on a damped primary structure, with components connected to both the primary and the base, is considered. We explore three elaborated cases depending on the grounded dampers distributing in the primary structure and the DVA. Our findings reveal that the frequency responses of the primary structure with dual resonant peaks of equal height may not be the global optimum, and we establish a nontrivial necessary condition for operable exact optimization. Furthermore, we elucidate the effects of structural arrangements on the optimized results and provide design rules to maximize vibration suppression performance. The optimization follows the proposal of a so-called resultant-based algorithm that guarantees global optimum with high efficiency and a generalizable core by exclusively constructing univariate polynomial equations. This study contributes a systematic analysis framework alongside efficient calculation tools for exact optimization and DVA performance evaluation.

1. Introduction

Dynamic vibration absorber (DVA) is a widely-used vibration reduction technique which was invented by Frahm [1] in the 1900s by attaching a proof mass to the primary structure via a spring, as depicted in Fig. 1(a). This undamped DVA prototype was shown to be effective in suppressing the vibrations at the natural frequency of the DVA itself. Den Hartog and Omondroyed [2] later introduced an additional damper to extend the vibration reduction band, leading to the damped DVA construction in Fig. 1(b). Furthermore, it showed that the frequency response curve of an un-damped primary structure crosses two fixed points regardless of the DVA damping, which can be used to optimize the stiffness and damping of the DVA to minimize the maximum motion amplitude of the primary, i.e., the so-called H_∞ optimization [3,4], resulting in the concept of tuned mass damper.

Based on the fixed-point theory and the H_∞ optimization criterion, extensive research has been conducted while proposing various DVA designs to further enhance performance. For instance, Ren [5] and Wong et al. [6,7] associated the damper of Den Hartog's DVA [2] with the base rather than the primary structure, and the optimized DVA exhibited superior performance. Krenk [8] proposed a root locus-based optimization procedure and additionally reduced DVA strokes and flattened the frequency response curve

* Corresponding author.
E-mail address: li.cheng@polyu.edu.hk (L. Cheng).

https://doi.org/10.1016/j.apm.2024.115812
Received 1 July 2024; Received in revised form 24 October 2024; Accepted 11 November 2024

Available online 2 December 2024

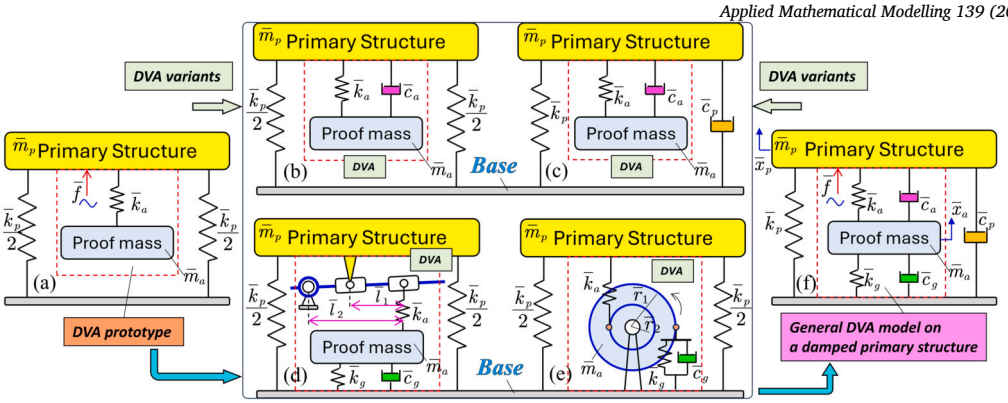

Fig. 1. (a). DVA prototype. (b). Den Hartog's DVA. (c). The DVA mounted on a damped primary structure. (d). Shen's lever-type DVA [30]. (e). Baduidana's flywheel-type DVA [31]. (f). The considered DVA model to be optimized.

of the primary structure by slightly increasing the optimal damping of Den Hartog's DVA. Cheung and Wong [9] and Li et al. [10] optimized DVA parameters and the installation position to reduce plate vibrations. Sun et al. [11–13] designed a tunable damper using the electromagnetic shunt to facilitate the practical implementation of optimum parameters. Moreover, negative grounded stiffness was introduced to Ren's DVA [5] with optimization and comparisons performed in [14]. Inerter components then showed benefits by achieving large-proof-mass effects and flexibility in connecting with other components [15–19]. The optimization of DVAs with both inerter and negative stiffness components can be referred to [20–23]. In addition, mechanical amplifying mechanisms are used to enhance vibration control, see [24–29] for broadband vibration absorption and isolation problems. For the H_∞ optimization problem of DVA, Shen et al. [30] combined the lever and negative-stiffness components as in Fig. 1(d) and showed that the lever component benefits vibration suppression in a way similar to an inerter. Following [30], Baduidana et al. [31] proposed and optimized a flywheel-type DVA depicted in Fig. 1(e) to simultaneously achieve the benefits of the lever and tunable inertia, resulting in further suppressed amplitude peaks of the primary structure and extended frequency band of vibration reduction, see also [32] for a similar flywheel-based DVA alternative. To handle the possible difficulties in connecting the DVA to the fixed ground, one can refer to [33–35] for skyhook dampers and electromagnetic solutions.

However, two issues are critical for the H_∞ optimization using the fixed-point method: (*i*). This method only gives approximate solutions. (*ii*). This method is unable to handle the cases where the primary structure is damped, exemplified by Fig. 1(b), (d), and (e). To tackle the latter problem, Asami et al. [36] took a further step using an approximate approach to seek series solutions. Thereafter, based on the DVA model in Fig. 1(c), Nishihara and Asami [37] proposed an exact method to adjust the two resonance peaks of the primary structure to the same height by using the relation between the polynomial coefficients and roots. The method, called Nishihara's method, yields exact closed-form and numerical solutions when the primary structure is undamped and damped, respectively. Following the same idea, Nishihara's method has now been generalized to the exact optimization of DVAs with multiple degrees of freedom (MDOF) and various combinations of springs and dampers [38–43].

Interestingly, we notice that existing studies use more the approximate fixed-point method to optimize DVAs rather than Nishihara's method, although the latter has presented exact solutions for over 20 years. Besides, the prerequisite for applying the fixed-point method is that the primary structure is either undamped or very slightly damped, which obviously leads to conservative results. Furthermore, to the best of our knowledge, even if the optimization problem is related to an undamped primary structure, which may hardly appear in engineering practice, none of the existing works that use the fixed-point method check if the considered DVAs can be exactly optimized before performing the approximate optimization. Thus, one main objective is to investigate the parametric conditions on the operability of exact optimization, an unexplored and crucial research gap.

Since the DVAs with grounded damping and stiffness are known to have better vibration suppression performance and since Nishihara's method is more used to optimize the DVA with all its components coupled between the proof mass and the primary structure, we here consider the exact optimization problem of a general DVA model as shown in Fig. 1(f), where the primary structure is damped and the DVA components are attached to both the base and the primary structure. Note that such a model is the prototype of a large range of DVA variants including the two in Fig. 1(d) and (e), given that the lever and flywheel essentially function as an inerter to alter DVA's equivalent proof mass [30,31]. That is, conclusions from this basic model can be generalized to guide the DVA design and optimization, as long as structural variants act as an alternation of equivalent system mass, stiffness, and damping, exemplified by the generalization of [38–43] from [37]. However, performing exact optimization is not a simple task since the increased number of DVA components makes the system dynamics more complex, especially considering that the term 'exact' means that we shall seek non-conservative analytical conditions to reach the global optimum.

We stress that only when simultaneously guaranteeing non-conservativeness, high efficacy, and ease of operation, can the exact methods be compelling when the approximate fixed-point method-based and exact optimization are both operable. This is related to the possible concerns that the improved performance by seeking exact solutions can be limited when the primary structure is undamped or slightly damped [37], while the equations to be handled for exact solutions become too complex to non-conservatively find the global optimum. To this end, we avoid the heavy iterative searching methods for optimizing complex structures [44–47]. Alternatively, we develop simplified exact optimization procedures inspired by Nishihara's method [37], i.e., equations to be handled

can be cast into purely polynomial forms. With this, the methods recently adopted by the authors for dynamical analysis [48–50], which convert a set of multivariable polynomial equations to much simpler univariate ones using the resultant concept [51], can be applied. Note that this idea has been partially reported in our previous work [52] for optimizing the DVA model in Fig. 1(c), but in a rudimentary and incomplete manner. Besides, the resultant concept also appeared in [37], where, however, only the reduced case with an undamped primary structure was considered. Based on the above, focusing on the general DVA model in Fig. 1(f), an automatic, purely algebraic, more efficient, and exact optimization algorithm is formally proposed in this work. Furthermore, the mentioned less-reported parametric effects of structural component arrangements on the optimization operability, solution behaviors, and vibration suppression are investigated and summarized. Particularly, issues with Nishihara's method when the primary structure is damped are discussed and complemented, a nontrivial necessary condition for an operable exact optimization is established for the first time, and counterexamples for the common belief that equal-peak feature yields the global optimum are found. This work systematically considers the exact optimization problem by characterizing solution behaviors and provides relevant general and efficient computational tools, with abundant comparison studies.

In what follows, Section 2 formulates the optimization problem. Sections 3, 4, and 5 address three elaborated optimization problems involving different damping arrangements to introduce the proposed optimization framework and its application and generalization. Section 6 presents the details and the efficiency of the proposed optimization procedures. Section 7 gives some further remarks on the optimization problem. Conclusions are drawn in Section 8. Italic symbols without a bar superscript '$\overline{\square}$' represent dimensionless quantities throughout the text.

2. Preliminaries

System dynamics and the optimization problem are formulated in this section. In particular, Nishihara's method [37] is formally refined as mathematical lemmas to facilitate further usages, with its essence highlighted.

2.1. Mathematical model

Dynamics of the 2DOF coupled system shown in Fig. 1(f), consisting of a primary structure, an absorber, and three pairs of linear springs and dampers, under the harmonic excitation $\bar{f}$, are governed by

$$\begin{bmatrix} \bar{m}_p & 0 \\ 0 & \bar{m}_a \end{bmatrix} \begin{bmatrix} \ddot{\bar{x}}_p \\ \ddot{\bar{x}}_a \end{bmatrix} + \begin{bmatrix} \bar{c}_p + \bar{c}_a & -\bar{c}_a \\ -\bar{c}_a & \bar{c}_a + \bar{c}_g \end{bmatrix} \begin{bmatrix} \dot{\bar{x}}_p \\ \dot{\bar{x}}_a \end{bmatrix} + \begin{bmatrix} \bar{k}_p + \bar{k}_a & -\bar{k}_a \\ -\bar{k}_a & \bar{k}_a + \bar{k}_g \end{bmatrix} \begin{bmatrix} \bar{x}_p \\ \bar{x}_a \end{bmatrix} = \begin{bmatrix} \bar{f} \\ 0 \end{bmatrix}, \tag{1}$$

where $\bar{x}_{(\cdot)}, \bar{m}_{(\cdot)}, \bar{c}_{(\cdot)}$, and $\bar{k}_{(\cdot)}$ represent displacement, mass, damping, and stiffness, respectively; the dotted symbols $\dot{\bar{x}}_{(\cdot)}$ and $\ddot{\bar{x}}_{(\cdot)}$ stand for the first- and the second-order derivatives with respect to time $\bar{t}$, respectively; in addition, the subscripts a, p, and g denote the absorber, the primary structure, and the grounded components, respectively. The governing equations (1) in the Laplace domain write

$$\begin{bmatrix} \bar{A}(\bar{s}) & \bar{B}(\bar{s}) \\ \bar{C}(\bar{s}) & \bar{D}(\bar{s}) \end{bmatrix} \begin{bmatrix} X_p \\ X_a \end{bmatrix} = \begin{bmatrix} F \\ 0 \end{bmatrix}, \tag{2}$$

where $\bar{s}$ is the Laplace variable such that $X_{p,a}(\bar{s}) = \mathscr{L}\left(\bar{x}_{p,a}(\bar{t})\right)$ and $F(\bar{s}) = \mathscr{L}\left(\bar{f}(\bar{t})\right)$, with the notation $\mathscr{L}(\cdot)$ denoting the Laplace transformation operation, and

$$\begin{cases} \bar{A}(\bar{s}) = \bar{m}_p \bar{s}^2 + \left(\bar{c}_p + \bar{c}_a\right)\bar{s} + \bar{k}_p + \bar{k}_a, \\ \bar{B}(\bar{s}) = -\left(\bar{c}_a \bar{s} + \bar{k}_a\right), \\ \bar{C}(\bar{s}) = -\left(\bar{c}_a \bar{s} + \bar{k}_a\right), \\ \bar{D}(\bar{s}) = \bar{m}_a \bar{s}^2 + \left(\bar{c}_a + \bar{c}_g\right)\bar{s} + \bar{k}_a + \bar{k}_g. \end{cases} \tag{3}$$

Introducing the following scaled symbols

$$\begin{aligned} &\mu = \bar{m}_a/\bar{m}_p, \bar{\omega}_p = \sqrt{\bar{k}_p/\bar{m}_p}, \bar{\omega}_a = \sqrt{\bar{k}_a/\bar{m}_a}, \eta = \bar{k}_g/\bar{k}_a, s = \bar{s}/\bar{\omega}_p, \\ &\upsilon = \bar{\omega}_a/\bar{\omega}_p, \zeta_p = \bar{c}_p/\left(2\bar{m}_p\bar{\omega}_p\right), \zeta_a = \bar{c}_a/\left(2\bar{m}_a\bar{\omega}_a\right), \zeta_g = \bar{c}_g/\left(2\bar{m}_a\bar{\omega}_a\right), \end{aligned} \tag{4}$$

the governing equation (2) can be reshaped into a dimensionless matrix form of

$$\mathbf{Z}\mathbf{X} = \mathbf{F} \tag{5}$$

where $\mathbf{X} = \left[X_p, X_a\right]^{\mathrm{T}}$, $\mathbf{F} = \left[F/\bar{k}_p, 0\right]^{\mathrm{T}}$, and

$$\mathbf{Z} = \begin{bmatrix} A(s) & B(s) \\ C(s) & D(s) \end{bmatrix}, \tag{6}$$

in which

$$\begin{cases} A(s) = s^2 + 2\zeta_p s + 1 + \mu\upsilon\left(2\zeta_a s + \upsilon\right), \\ B(s) = -\mu\upsilon\left(2\zeta_a s + \upsilon\right), \\ C(s) = -\upsilon\left(2\zeta_a s + \upsilon\right), \\ D(s) = s^2 + \upsilon\left(2\zeta_g s + \eta\upsilon\right) + \upsilon\left(2\zeta_a s + \upsilon\right). \end{cases} \tag{7}$$

Consequently, the transfer function between the displacement $\bar{x}_p$ of the primary structure and the force excitation $\bar{f}$ is

$$G_{F\mapsto X_p}(s) = \frac{X_p(s)}{F(s)/\bar{k}_p} = \mathbf{Z}^{-1}_{(1,1)} = \frac{n(s)}{d(s)}, \tag{8}$$

where $\mathbf{Z}^{-1}_{(1,1)}$ represents the $(1,1)$ element of $\mathbf{Z}^{-1}$, and $n(s)$ and $d(s)$ are polynomials in s. Furthermore, the amplitude magnification factor (AMF) concerning the primary structure at the dimensionless excitation frequency $\omega = \bar{\omega}/\bar{\omega}_p \geqslant 0$ is defined as

$$A(\omega) = \left|G_{F\mapsto X_p}(s = j\omega)\right| = \left|\frac{n(s = j\omega)}{d(s = j\omega)}\right| = \sqrt{\frac{N(\Omega)}{D(\Omega)}}, \tag{9}$$

where $j = \sqrt{-1}$, $N(\Omega)$ and $D(\Omega)$ are two polynomials in $\Omega = \omega^2$.

2.2. Formulation of the exact H_∞ optimization problem

From (7), six parameters $\boldsymbol{\vartheta}_{all} = \left(\mu, \eta, \upsilon, \zeta_p, \zeta_a, \zeta_g\right)$ can be theoretically manipulated to enhance vibration suppression performance. The H_∞ optimization criterion is adopted for the optimal DVA design to minimize the maximum amplitude of residual vibrations on the primary structure. The procedure starts with defining the H_∞ norm

$$h = \|A(\omega)\|_\infty = \max\{A(\omega)\}, h > 1, \tag{10}$$

and the goal is to seek the parameter composition that minimizes h to achieve the minimum denoted as $h_{\min}$. The frequencies corresponding to the peaks of the AMF $A(\omega)$ are referred to as resonance frequencies, leading to Proposition 1.

Proposition 1 *(Exactly optimized AMF (EO-AMF)). The EO-AMF has two peaks of an identical minimum height $h_{\min}$ so that $A\left(\omega_A\right) \equiv A\left(\omega_B\right) = h_{\min}$, where ω_A and ω_B are the two resonance frequencies. We let $0 < \omega_A < \omega_B$.* □

Definition 1 *(Potentially optimized AMF (PO-AMF)).* Any AMF curve exhibiting two peaks at an identical peak height h, i.e., $A\left(\omega_A\right) \equiv A\left(\omega_B\right) = h$, is defined as the PO-AMF. □

Remark 1. Proposition 1 stipulates that the optimization is to achieve two exactly equal resonance peaks (i.e., the so-called equal-peak optimization in [44,45,47]), indicating that the optimization is based on the typical feature of 2DOF dynamics. That is, we exclude the reduced cases where the DVA has a heavy stiffness $\bar{k}_a$ and grounded damping $\bar{c}_g$ so that the coupled system acts like an SDOF structure with one resonance peak [6]. Such cases may lead to a smaller $h_{\min}$ but compromise the reduced efficacy of vibration suppression (i.e., $A < 1$) and the high costs of mechanical components in practice. □

Clearly, all parameter compositions $\boldsymbol{\vartheta}_{all}$ corresponding to the EO-AMF form a subset of those to the PO-AMF. The following two preliminary lemmas are summarized in light of Nishihara's method [37].

Lemma 1. *For any PO-AMF with a peak amplitude h, the squares of its two resonance frequencies, i.e., $\Omega_A = \omega_A^2$ and $\Omega_B = \omega_B^2$, must be the two real double roots of a quartic polynomial equation in Ω*

$$Q(\Omega, h) = h^2 D(\Omega) - N(\Omega) = \sum_{i=0}^{4} a_i(h)\,\Omega^i = 0, \tag{11}$$

where $a_i, i = 0, 1, 2, 3, 4$ are polynomials in h. Notably, $a_0 = \upsilon^4\left[\left(\mu\eta\upsilon^2 + \eta + 1\right)^2 h^2 - (\eta + 1)^2\right]$ and $a_4 = h^2$.

Proof. Combining Eqs. (9) and (10), the relationship between $\Omega_{A,B}$ and h satisfies

$$Q(\Omega, h) = h^2 D(\Omega) - N(\Omega) = 0. \tag{12}$$

Besides, the independence condition of the peak h concerning Ω, i.e., $dh/d\Omega = 0$, enforces

$$\frac{dQ(\Omega, h)}{d\Omega} = \frac{\partial Q(\Omega, h)}{\partial h}\frac{\partial h}{\partial \Omega} + \frac{\partial Q(\Omega, h)}{\partial \Omega} = h^2\frac{\partial D(\Omega)}{\partial \Omega} - \frac{\partial N(\Omega)}{\partial \Omega} = 0. \tag{13}$$

Considering also that $Q(\Omega, h) = 0$ is a quartic polynomial equation and it only has two real positive roots Ω_A and Ω_B for the PO-AMF as per Definition 1, Ω_A and Ω_B then must be the two double roots of this equation. □

Lemma 2. *If $\eta = 0$, any composition ϑ_{all} yielding the PO-AMF must be a common solution of the two equations*

$$\begin{cases} f_1\left(r, \vartheta_{all}\right) = b_3\sqrt{b_0} - b_1 = 0, \\ f_2\left(r, \vartheta_{all}\right) = \frac{b_3^2}{4} + 2\sqrt{b_0} - b_2 = 0, \end{cases} \tag{14}$$

where $b_i, i = 0, 1, 2, 3$ are polynomials parameterized in $\left(r, \vartheta_{all}\right)$, see (18) in proof for the relevant definitions.

Proof. Letting $\eta = 0$ and defining

$$r^2 = \frac{h^2 - 1}{h^2}, 0 < r < 1, \tag{15}$$

Eq. (11) can be simplified into a monic quartic polynomial equation as

$$Q\left(\Omega, h\right) \xrightarrow{\eta=0} Q_{sim}\left(\Omega, r\right) = \sum_{i=0}^{4} b_i \Omega^i = 0, \tag{16}$$

where $b_0 = r^2 v^4$ and $b_4 = 1$, see also the forms of the two coefficients a_0 and a_4 in Eq. (11) for comparisons. Furthermore, if Eq. (16) has two double roots Ω_A and Ω_B for the parameter composition yielding the PO-AMF as per Lemma 1, it satisfies

$$Q_{sim}\left(\Omega, r\right) = \left(\Omega - \Omega_A\right)^2 \left(\Omega - \Omega_B\right)^2, \tag{17}$$

leading to

$$\begin{cases} b_4 = 1, b_3 = -2\left(\Omega_A + \Omega_B\right), \\ b_2 = \Omega_A^2 + 4\Omega_A\Omega_B + \Omega_B^2, \\ b_1 = -2\Omega_A\Omega_B\left(\Omega_A + \Omega_B\right), b_0 = \Omega_A^2\Omega_B^2. \end{cases} \tag{18}$$

Combining the coefficients in (18) leads to the two equations in (14), thus completing the proof. □

Remark 2. Given $\partial r / \partial h > 0$ as per (15), the optimization problem is to seek the point corresponding to the global minimum of r on the intersection line of the two surfaces governed by the solutions of the two equations in (14). □

2.3. Issues on Nishihara's method

The essential kernel of Nishihara's method is Lemma 2, which confines all the parameter compositions yielding the PO- or the EO-AMF to the common solutions of two polynomial equations that are independent of resonance frequencies. To optimize the parametric pair of $\vartheta = \left(v, \zeta_a\right) \in \vartheta_{all}$ in the reduced case $\left(\zeta_p, \zeta_g, \eta\right) = (0, 0, 0)$ as in Fig. 1(b), the two equations in (14) can be integrated into a binary polynomial equation with the highest degree of four [37], and the variables can be further eliminated, yielding a quadratic polynomial equation so that closed-form solutions are available. If the primary structure is damped with $\zeta_p > 0$ as in Fig. 1(c), Nishihara's method constructs an auxiliary equation by calculating the Jacobian matrix

$$\mathbf{J}\left(r, \vartheta\right) = \frac{\partial\left(f_1\left(r, \vartheta\right), f_2\left(r, \vartheta\right)\right)}{\partial \vartheta}. \tag{19}$$

The minimum condition of r enforces $\mathbf{J}\left(r, \vartheta\right)$ to be singular so that the number of equations obtained is equal to the number of the unknowns (r, ϑ), and thus the optimal parameter pair $\left(v, \zeta_a\right)$ can be numerically solved.

However, solving multiple variables from multiple nonlinear (even polynomial) equations is not trivial, and obviously, the solution convergence highly depends on proper initial guesses [37,42]. On the other hand, such a brute-force numerical procedure can be conservative due to the lack of prior knowledge that the common solution corresponding to the singularity of (19) must yield the global minimum of r [52]. Addressing such issues is one of the targets of the proposed optimization procedure.

2.4. Operable polynomial-based optimization and two complementary lemmas

Note that $\eta = 0$ is the prerequisite for a polynomial-based optimization procedure. Otherwise, the term $\sqrt{b_0}$ in Lemma 2 is irrational given the form of the coefficient a_0 in Eq. (11). Since r is included in b_0 and since we are seeking its analytical extremum condition with respect to the parameter composition ϑ_{all}, the irrational form of $\sqrt{b_0}$ when $\eta \neq 0$ implies that the mathematical properties of the polynomial equations cannot be used, and therefore the pure numerical seeking procedure becomes the only option. Hence, the condition $\eta = 0$ holds in what follows to demonstrate the benefits of the polynomial forms, which agrees with the purpose of this work to establish an efficient and non-conservative exact optimization procedure. The challenges of the exact optimization when $\eta \neq 0$ are discussed in Section 7.

Next, a preparatory Lemma 3 is given to exclude the infeasible common solutions of Eq. (14). Lemma 4 directly determines the two resonance frequencies $\left(\omega_A, \omega_B\right)$, thus simplifying the procedure in [37]. Note that the fixed-point method cannot analytically determine the resonance frequencies.

Lemma 3. *If $\eta = 0$, any parameter composition ϑ_{all} that yields the PO-AMF must satisfy*

$$f_3\left(r, \vartheta_{all}\right) = 6b_3b_0 - b_2b_1 \neq 0, \tag{20}$$

where b_i are the polynomial coefficients defined in Eq. (16).

Proof. The common solutions of Eq. (14) are expected to assign two double roots Ω_A and Ω_B to (16), so we exclude the reduced case where Eq. (16) has a quartic root $\Omega = \Omega_A = \Omega_B$, which leads to

$$Q(\Omega) = \sum_{i=0}^{4} b_i\Omega^i = \left(\Omega - \Omega_A\right)^4 = 0. \tag{21}$$

The coefficients b_i in this reduced case satisfy

$$\begin{cases} b_4 = 1, b_3 = -4\Omega_A, \\ b_2 = 6\Omega_A^2, b_1 = -4\Omega_A^3, b_0 = \Omega_A^4, \end{cases} \tag{22}$$

which can be combined into

$$6b_3b_0 - b_2b_1 = 0. \tag{23}$$

Thus, any parameter composition ϑ_{all} that renders Eq. (16) two double roots must contradict the condition (23). □

Lemma 4. *If $\eta = 0$, the two resonance frequencies of any PO-AMF, ω_A and ω_B, $0 < \omega_A < \omega_B$, are governed by*

$$\omega_{A,B} = \frac{1}{4}\sqrt{-\frac{b_3}{2} \mp \sqrt{b_2 - 6\sqrt{b_0}}}, \tag{24}$$

where b_i are the polynomial coefficients defined in Eq. (16).

Proof. The two resonance frequencies correspond to the two double roots of Eq. (16). From (18), we have

$$\begin{cases} \Omega_A + \Omega_B = -b_3/2, \\ \Omega_A - \Omega_B = -\sqrt{b_2 - 6\sqrt{b_0}}. \end{cases} \tag{25}$$

Solving Eq. (25) given the transforms $\omega_A = \sqrt{\Omega_A}$ and $\omega_B = \sqrt{\Omega_B}$ completes the proof. □

2.5. Operable polynomial-based optimization and two complementary lemmas

Even with η excluded, simultaneously optimizing the remaining five parameters $\left(\mu, \upsilon, \zeta_p, \zeta_a, \zeta_g\right)$ is still impractical. The damping ratio ζ_p is inherent in the primary structure, and so is the mass ratio μ for a given absorber mass $\bar{m}_a$, and thus we take $\left(\zeta_p, \mu\right)$ as known. The optimization handles the three parameters $\left(\upsilon, \zeta_a, \zeta_g\right)$ that correspond to the stiffness and damping of the DVA. Noting from (15) that $\partial r/\partial h > 0$ and denoting the optimum parameter composition for $h_{\min}$ or equivalently $r_{\min}$ as $\left(\upsilon_{opt}, \zeta_{a,opt}, \zeta_{g,opt}\right)$, the exact H_∞ optimization problem can be formulated as

$$\begin{pmatrix} \upsilon_{opt} \\ \zeta_{a,opt} \\ \zeta_{g,opt} \end{pmatrix}^{\mathrm{T}} = \left\{ \min_{\upsilon,\zeta_a,\zeta_g} \{r\}, s.t. : \begin{Bmatrix} 0 < r < 1 \\ f_1\left(r, \upsilon, \zeta_a, \zeta_g\right) = 0 \\ f_2\left(r, \upsilon, \zeta_a, \zeta_g\right) = 0 \\ f_3\left(r, \upsilon, \zeta_a, \zeta_g\right) \neq 0 \end{Bmatrix} \right\}. \tag{26}$$

That is, we seek the composition $\left(r_{\min}, \upsilon_{opt}, \zeta_{a,opt}, \zeta_{g,opt}\right)$. The reduced case without grounded dampers, i.e., $\zeta_p = \zeta_g = 0$, is well tackled in [37] with closed-form solutions and thus is not considered. We focus on how the two grounded damping ζ_p and ζ_g affect optimization and vibration suppression. Three cases $\left(\zeta_p > 0, \zeta_g = 0\right)$, $\left(\zeta_p = 0, \zeta_g > 0\right)$, and $\left(\zeta_p > 0, \zeta_g > 0\right)$, are elaborated for demonstration. Accordingly, the superscript $(\cdot)^{[i]}$ representing Case $i, i = 1, 2, 3$, is used for discrimination.

3. Case 1: grounded damping only in the primary structure ($\zeta_p > 0, \zeta_g = 0$)

Closed-form solutions are inaccessible once the primary structure is damped, and the fixed-point method cannot handle this case. To avoid the direct procedure of Nishihara's method that incorporates the Jacobian matrix (19) for numerical solutions, our recent works [48–50,52] adopted a Sylvester resultant-based procedure to construct purely univariate polynomial equations. Such a procedure is complemented and modified here using the Dixon resultant concept [53–57] for higher efficiency to cope with the more complex DVA model and is further studied to establish a nontrivial necessary condition for an operable exact optimization. The significantly improved efficiency is detailed in Section 6 by comparisons.

3.1. Equations to be handled

The two variables to be optimized are (v, ζ_a), and the common solutions of Eq. (14) are required for optimization. Taking $f_1(r, v, \zeta_a) = 0$ and $f_2(r, v, \zeta_a) = 0$ as two polynomial equations in ζ_a (a similar procedure holds if starting with v) yields

$$\begin{cases} f_{1,[r,v]}^{[1]}(\zeta_a) = \sum_{i=0}^{2} \alpha_i^{[1]}(r, v)\, \zeta_a^i = 0, \\ f_{2,[r,v]}^{[1]}(\zeta_a) = \sum_{i=0}^{4} \beta_i^{[1]}(r, v)\, \zeta_a^i = 0, \end{cases} \tag{27}$$

where $\alpha_i^{[1]}$ and $\beta_i^{[1]}$ are polynomial coefficients in (r, v), and the factor $2v^2$ corresponding to $v = 0$ of Eq. (27) has been excluded for simplicity. Denoting the highest degree of the variable λ in the polynomial p as $deg[p, \lambda]$, we have $\max\left\{deg\left[\alpha_i^{[1]}, v\right]\right\} = 2$ and $\max\left\{deg\left[\beta_i^{[1]}, v\right]\right\} = 4$. Note that no analytical common solutions of Eq. (27) exist due to the increased equation degrees and the coupling between variables. To avoid numerical solutions, we introduce Dixon resultant [55].

3.2. Dixon resultant concept

Dixon resultant is a concept that seeks the necessary condition for two polynomial equations to have common solutions. The Dixon resultant-based optimization procedure starts with constructing the Dixon polynomial,

$$\delta(\zeta_a, \wp) = \frac{1}{\zeta_a - \wp} \begin{vmatrix} f_{1,[r,v]}^{[1]}(\zeta_a) & f_{2,[r,v]}^{[1]}(\zeta_a) \\ f_{1,[r,v]}^{[1]}(\zeta_a = \wp) & f_{2,[r,v]}^{[1]}(\zeta_a = \wp) \end{vmatrix}, \tag{28}$$

where $\wp$ represents an auxiliary symbol, and the highest degree of δ in $\wp$ is $d_{\max} - 1 = 3$, with

$$d_{\max} = \max\left\{deg\left[f_{1,[r,v]}^{[1]}, \zeta_a\right], deg\left[f_{2,[r,v]}^{[1]}, \zeta_a\right]\right\}. \tag{29}$$

From the construction of Eq. (28), $\delta(\zeta_a, \wp) = 0$ holds at each common solution ζ_a of $f_{1,[r,v]}^{[1]}(\zeta_a) = 0$ and $f_{2,[r,v]}^{[1]}(\zeta_a) = 0$ regardless of the $\wp$ values. Hence, all the coefficients of $\wp^i$, $i = 0, 1, \cdots d_{\max} - 1$, must vanish at this solution resulting in $d_{\max}$ equations, which can be written in a matrix form of

$$\mathbf{D}(r, v) \begin{bmatrix} 1 \\ \zeta_a \\ \vdots \\ \zeta_a^{d_{\max}-1} \end{bmatrix} = \mathbf{0}, \tag{30}$$

where the coefficient matrix $\mathbf{D}(r, v)$ is known as the Dixon matrix. Clearly, $\mathbf{D}(r, v)$ needs to be singular for Eq. (27) to have common solutions of ζ_a, leading to a polynomial equation in (r, V),

$$\mathcal{D}_{\zeta_a}\left(f_{1,[r,v]}^{[1]}(\zeta_a), f_{2,[r,v]}^{[1]}(\zeta_a)\right) = |\mathbf{D}(r, v)| = V^4 R_1^{[1]}(r, V) = 0, \tag{31}$$

where $V = v^2$, $R_1^{[1]}$ is a polynomial in (r, V), the determinant $|\mathbf{D}(r, v)|$ is known as the Dixon resultant, and the notation $\mathcal{D}_\lambda(p_1, p_2)$ is used to denote the Dixon resultant operation between two polynomial equations p_1 and p_2 to eliminate λ. Consequently, any common solution ζ_a of Eq. (27) must correspond to at least one solution pair (r, v) of Eq. (31), but the reverse is not the case since $|\mathbf{D}(r, v)| = 0$ holds if all the coefficients of ζ_a^i in either one of the two equations in (27) are zero, so the Dixon resultant provides a necessary condition for common solutions.

Remark 3. The core of the resultant concept is that two multivariate polynomial equations are transformed into a single equation where one variable is eliminated. In addition, the solutions (in terms of the kept variables) of the transformed equation contain those of the original set of equations. □

Remark 4. From (30), for two polynomials with their degrees respectively denoted as d_1 and d_2, the resulting Dixon matrix $\mathbf{D}$ has the dimension of $d_{\max} \times d_{\max}$, where $d_{\max} = \max\{d_1, d_2\}$, while the dimension of the corresponding widely adopted Sylvester matrix labeled by $\mathbf{S}$ is $(d_1 + d_2) \times (d_1 + d_2)$, see also a brief comparison between such two resultant concepts in Appendix. A smaller dimension of the Dixon matrix means higher computational efficiency and the benefit better shows off as system dynamics become more complex, as to be demonstrated through experimental comparisons in Section 6.1. □

3.3. Dixon resultant-based optimization procedure

Deploying one Dixon resultant operation by eliminating ζ_a arrives at Eq. (31), a bivariate polynomial equation containing all the common solutions (r, V) of Eq. (27) regardless of ζ_a. Since $V \neq 0$, Eq. (31) is reduced to

$$R_1^{[1]}(r,V)=\sum_{i=0}^{8}\gamma_i^{[1]}(r)V^i=0, \tag{32}$$

where $\gamma_i^{[1]}$ are polynomial coefficients in r. The differential form of (32) is

$$dR_1^{[1]}(r,V)=\frac{\partial R_1^{[1]}(r,V)}{\partial r}dr+\frac{\partial R_1^{[1]}(r,V)}{\partial V}dV=0. \tag{33}$$

Therefore, the extremum condition of r with respect to υ can be converted as

$$\begin{aligned}\frac{\partial r}{\partial \upsilon}=0\rightarrow\frac{\partial r}{\partial V}=0\\ \rightarrow\frac{\partial R_1^{[1]}(r,V)}{\partial V}=\sum_{i=0}^{7}(i+1)\gamma_{i+1}^{[1]}(r)V^i=0.\end{aligned} \tag{34}$$

The desired minimum $r_{\min}^{[1]}$ and the associated $\left(\upsilon_{opt}^{[1]}\right)^2$ must be the common solution of Eqs. (32) and (34). Then, one more resultant operation similar to Eq. (31) can be deployed, yielding the so-called discriminant [58] of the resultant Eq. (32)

$$\begin{aligned}R_{2,0}^{[1]}(r)&=\mathcal{D}_V\left(R_1^{[1]}(r,V),\frac{\partial R_1^{[1]}(r,V)}{\partial V}\right)\\&=(r+1)^4(r-1)^6r^{60}R_2^{[1]}(r)=0.\end{aligned} \tag{35}$$

Since $r\in(0,1)$, any extremum of r with respect to υ must satisfy

$$R_2^{[1]}(r)=\sum_{i=0}^{46}\kappa_i^{[1]}r^i=0, \tag{36}$$

which is a univariate polynomial equation in r only, where $\kappa_i^{[1]}$ are real constant coefficients.

Remark 5. By deploying resultant operations twice, the minimum condition of r with respect to (υ,ζ_a), i.e.,

$$\begin{cases}\frac{\partial r}{\partial \upsilon}=0 and\ \frac{\partial r}{\partial \zeta_a}=0, or\\ dr=\frac{\partial r}{\partial \upsilon}d\upsilon+\frac{\partial r}{\partial \zeta_a}d\zeta_a=0,\end{cases} \tag{37}$$

is reduced to solving a univariate polynomial equation (36) whose solutions contain all extrema of r with respect to υ. Clearly, the global minimum $r_{\min}^{[1]}$ satisfying (37) must be a solution of Eq. (36). Such a simplification is the key to our resultant-based procedure to avoid the pure numerical procedure of Nishihara's method, as mentioned in Section 2.3. □

With the univariate form of Eq. (36), a nontrivial necessary condition of an operable exact optimization problem can be established, given that the solutions of a univariate polynomial equation can be exhaustively determined by regular routines without the need for initial guess, such as calculating the standard QR decomposition and companion matrix [59], leading to Theorem 1, which presents a useful tool to check if the DVA is exactly optimizable.

Theorem 1 *(Operable exact H_∞ optimization problem). If the univariate polynomial equation $R_2^{[1]}(r)=0$ has no real solution satisfying $r\in(0,1)$, then no parameter pair $\left(\upsilon_{opt}^{[1]},\zeta_{a,opt}^{[1]}\right)$ exists such that the AMF $A(\omega)$ has two peaks of an identical height. That is, no solutions to the exact H_∞ optimization problem exist for the EO-AMF.* □

Proceeding from Eq. (36), the exhaustive solutions of this univariate polynomial equation are collected as

$$\mathbf{r}^{[1]}=\left\{r|R_2^{[1]}(r)=0,0<r<1\right\}. \tag{38}$$

Substituting each $r\in\mathbf{r}$ into Eq. (32) or (34) yields a polynomial equation in V only, and thus the associated natural frequency ratio υ can be exhaustively solved. Similarly, plugging each obtained solution pair (r,υ) into either of the two equations in (27) gives a univariate polynomial equation in the damping ζ_a. By doing so, the solving process handles purely univariate polynomial equations that can be easily solved. More intuitively, such an optimization procedure is demonstrated in Fig. 2, in which two parameters (ϑ,i) need to be specified before executing the procedure in Fig. 2. Particularly, ϑ signifies the damping ratio to be optimized, and the other one i is related to Case i, e.g., $(\vartheta,i)=(a,1)$ is selected for Case 1.

The noteworthy aspects of the optimization procedure proposed in Fig. 2 are highlighted as follows. First, the solutions of $R_2^{[i]}(r)=0$, which are $r_{[m]}$, $r_{[m]}\in\mathbf{r}$, are substituted into the equation $\partial R_1^{[i]}(r,V)/\partial V=0$ instead of $R_1^{[i]}(r,V)=0$ for solution V in step ② since

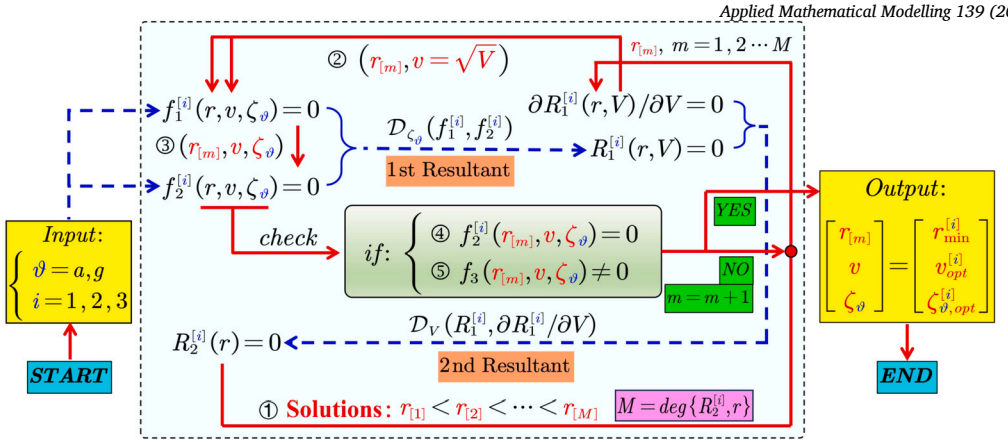

Fig. 2. Univariate polynomial equation-based exact H_∞ optimization using the Dixon resultant concept. Blue dashed arrows represent the preparatory steps, and red solid ones are the main steps of the solving process.

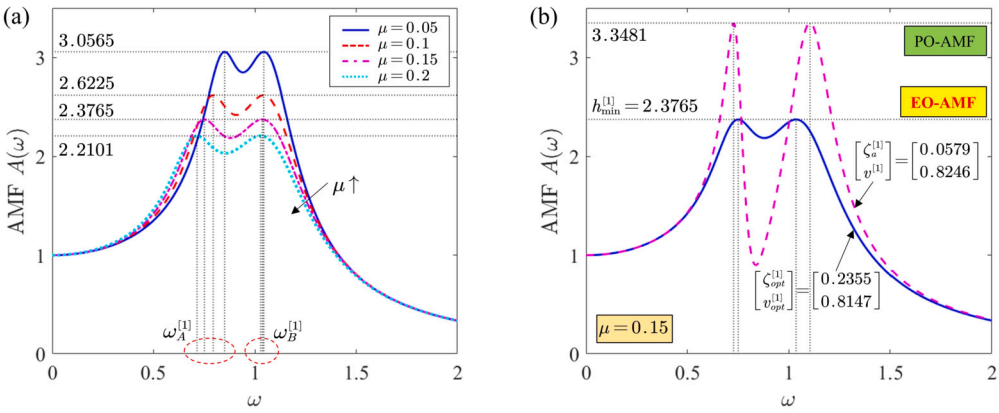

Fig. 3. (a). The EO-AMF with respect to μ for $\zeta_p = 0.1$. The resonance frequencies $\left(\omega_A^{[1]}, \omega_B^{[1]}\right)$ are calculated following Lemma 3. (b). Two PO-AMFs with $\mu = 0.15$.

the former equation is of a lower degree. Similarly, the pair $(r_{[m]}, v)$, which is the solution of $\partial R_1^{[i]}(r, V)/\partial V = 0$, is plugged into $f_1^{[i]}(r, v, \zeta_\vartheta) = 0$ for solutions of ζ_ϑ in step ③. Besides, all three solving steps denoted as ①, ②, and ③ handle univariate polynomial equations. Given that the resultant concept only provides a necessary condition for common solutions as introduced in Section 3.2 and Lemma 3 needs to be additionally satisfied, the two checking steps ④ and ⑤ are finally deployed. Clearly, the first returned solution composition must be the global optimum since the solving process is performed in the ascending order of $r \in \mathbf{r}$. This is a generalizable algorithm, and its easy application in the other two cases is demonstrated in Sections 4 and 5.

3.4. Verification and discussion

Selecting $\zeta_p = 0.1$, the EO-AMF for four different mass ratios $\mu = [0.05, 0.1, 0.15, 0.2]$ are compared in Fig. 3(a), with the associated parameters tabulated in Table 1.

From Fig. 3(a), all the EO-AMF curves exhibit two peaks of an identical height and the associated resonance frequencies $\left(\omega_A^{[1]}, \omega_B^{[1]}\right)$ concur with Lemma 4, thus verifying the theoretical analysis. Moreover, increasing the mass ratio μ reduces the optimized peak height $h_{\min}^{[1]}$, which agrees with [30,31], where lever and flywheel constructions enhance vibration suppression performance by increasing DVA's inertia. However, one should notice the marginal effect of such performance enhancement. That is, a much larger increase in μ is required for the same reduction of $h_{\min}^{[1]}$ as μ increases, meaning that a large absorber mass $\bar{m}_a$ is required for a given primary structure with a fixed mass $\bar{m}_p$, or more complicated constructions are required to alter the DVA's inertia. To this end, we should have all components that benefit vibration suppression in effect to achieve a desirably low value of the peak h in case only deploying one of them complicates the mechanical design and assembly.

On the other hand, note from Fig. 2 that all the parameter pairs (v, ζ_a) satisfying the extremum condition $\partial r/\partial v = 0$ can be determined if we do not quit this algorithm as it gives the first output, and then collect all solution compositions that pass the 'YES' channel. Taking $\mu = 0.15$ as an example yields Fig. 3(b), where two PO-AMF curves co-exist, each of which corresponds to a local extremum of r. Clearly, the AMF at the smallest peak height is the EO-AMF, as marked in Fig. 3(b). This example demonstrates how the resultant-based optimization procedure in Fig. 2 guarantees the global optimum. Recall from Section 2.3 that Nishihara's method

Table 1
Parameters associated with Fig. 3(a).

μ	$h_{\min}^{[1]}$	$r_{\min}^{[1]}$	$\left(\upsilon_{opt}^{[1]},\zeta_{a,opt}^{[1]}\right)$	$\left(\omega_A^{[1]},\omega_B^{[1]}\right)$
0.05	3.0566	0.9450	(0.9138, 0.1475)	(0.8508, 1.0441)
0.10	2.6225	0.9244	(0.8619, 0.1988)	(0.7944, 1.0431)
0.15	2.3765	0.9071	(0.8174, 0.2355)	(0.7509, 1.0367)
0.20	2.2101	0.8918	(0.7780, 0.2645)	(0.7145, 1.0283)

when $\zeta_p > 0$ simultaneously solves multiple nonlinear equations based on the singularity of the Jacobian matrix (19). Hence, the solution obtained may not correspond to the global minimum of r and, conversely, can even yield a maximum due to the lack of prior knowledge that the optimum composition is the unique solution of such multiple nonlinear equations. This observation, namely, the AMF curves with two peaks of an identical height may not be optimum, provides possible counterexamples for the optimizations that are only based on the equal-peak property, which is an important issue absent in the open literature [44,45,47]. Accordingly, one can conclude that the equal-peak optimization only provides a necessary but not sufficient condition for the global optimum, signifying the core benefits of modifying Nishihara's method for seeking analytical global optimum conditions.

4. Case 2: grounded damping only in the DVA $\left(\zeta_p = 0, \zeta_g > 0\right)$

Having established the Dixon resultant-based optimization procedure in Case 1, we here generalize it to another optimization problem where the grounded damper is only associated with the DVA so $\zeta_p = 0$ and $\zeta_g > 0$. Existing studies [30,31] show that approximate optima of $\left(\upsilon,\zeta_g\right)$ via the fixed-point method are available when $\zeta_a = 0$. Thus, depending on the existence of ζ_a, the discussions are divided into two aspects to exactly optimize $\left(\upsilon,\zeta_g\right)$ for comparisons.

4.1. Equations to be handled

This time, Eq. (14) is parameterized in $\left(r,\upsilon,\zeta_g\right)$ and is separated into two polynomial equations in ζ_g in light of Section 3.1 and Fig. 2. When $\zeta_a \neq 0$, we have

$$\begin{cases} f_{1,[r,\upsilon]}^{[2]}\left(\zeta_g\right) = \sum_{i=0}^{2} \alpha_i^{[2]}\left(r,\upsilon\right)\zeta_g^i = 0, \\ f_{2,[r,\upsilon]}^{[2]}\left(\zeta_g\right) = \sum_{i=0}^{4} \beta_i^{[2]}\left(r,\upsilon\right)\zeta_g^i = 0, \end{cases} \tag{39}$$

where $\alpha_i^{[2]}$ and $\beta_i^{[2]}$ are real polynomial coefficients in (r,υ), and $\max\left\{deg\left[\alpha_i^{[2]},\upsilon\right]\right\} = \max\left\{deg\left[\beta_i^{[2]},\upsilon\right]\right\} = 4$. Note that the grounded damping ζ_g arises the degree of υ in $\alpha_i^{[2]}$ compared with the previous Case 1, and thus starting the resultant-based optimization procedure with eliminating ζ_g instead of υ benefits efficiency as per Remark 4.

With Eq. (39), selecting $(\vartheta,i) = (g,2)$ in Fig. 2 yields the optimization procedure for the optimum composition $\left(r_{\min}^{[2]},\upsilon_{opt}^{[2]},\zeta_{g,opt}^{[2]}\right)$. Specifically, the forms of the two intermediate resultant equations are signified,

$$\begin{cases} R_1^{[2]}\left(r,V\right) = simplify\left(\mathcal{D}_{\zeta_g}\left(f_1^{[2]},f_2^{[2]}\right)\right) = \sum_{i=0}^{12}\gamma_i^{[2]}\left(r\right)V^i = 0, \\ R_2^{[2]}\left(r\right) = simplify\left(\mathcal{D}_V\left(R_1^{[2]},\frac{\partial R_1^{[2]}}{\partial V}\right)\right) = \sum_{i=0}^{70}\kappa_i^{[2]}r^i = 0, \end{cases} \tag{40}$$

where $\gamma_i^{[2]}$ are polynomial coefficients in r, $\kappa_i^{[2]}$ are real constants, and the notation $simplify(\cdot)$ represents excluding the factors corresponding the inappropriate solutions satisfying $V \leqslant 0$ and $r \notin (0,1)$.

Remark 6. The required minor changes of the Dixon resultant-based optimization algorithm in Fig. 2 in input when handling Cases 1 and 2 benefit from the generalizable core of this algorithm for all polynomial-based optimizations. □

4.2. Optimization and comparisons when $\zeta_a = 0$

In the reduced case $\zeta_a = 0$, Ren [5] derived the approximately optimized pair of $\left(\upsilon,\zeta_g\right)$ via the fixed-point method

$$\tilde{\upsilon}_{FP}^{[2]} = \sqrt{\frac{1}{1-\mu}}, \tilde{\zeta}_{g,FP}^{[2]} = \sqrt{\frac{3\mu}{4\left(2-\mu\right)}}, \tag{41}$$

where the superscript '$\widetilde{\square}$' represents the reduced case and the subscript $(\cdot)_{FP}$ means the fixed-point method for discrimination. The exact solutions are considered for comparisons. Substituting $\zeta_a = 0$ into Eqs. (39) yields

$$\begin{cases} \tilde{f}_{1,[r,\upsilon]}^{[2]}\left(\zeta_g\right) = 2\left(\left(r-2\mu\right)V - r^2 - \mu^2V^2\right)Z_g + \left(1-r\right)\left(1+\mu\right)V + r\left(r-1\right) = 0, \\ \tilde{f}_{2,[r,\upsilon]}^{[2]}\left(\zeta_g\right) = 4V^2Z_g^2 + 4V\left(\left(\mu-1\right)V+4\right)Z_g + 1 + 2\left(r-1\right)V - r^2 = 0, \end{cases} \tag{42}$$

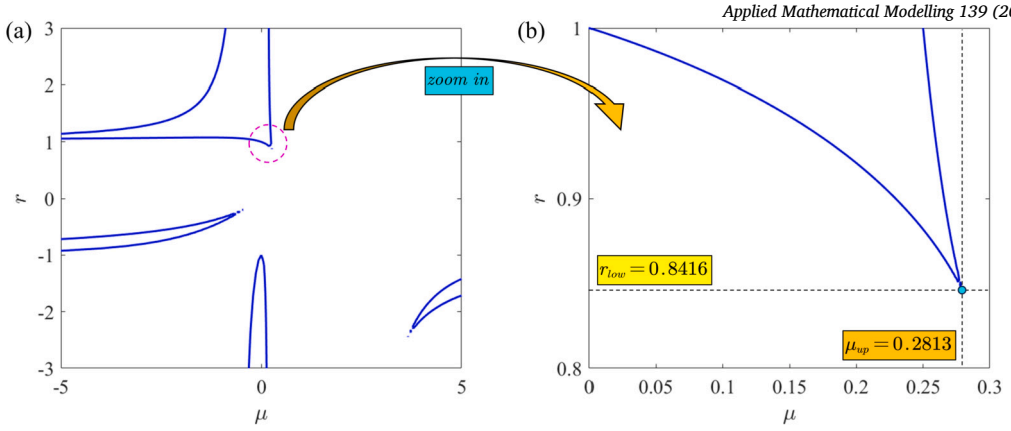

Fig. 4. (a). The implicit relationship between μ and r governed by Eq. (43). (b). The zoomed plot of (a) for $\mu > 0$.

Table 2
Parameters associated with Fig. 5(a).

μ	EO-AMF			Approximately optimized AMF	
	$\tilde{h}^{[2]}_{\min}$	$\left(\tilde{v}^{[2]}_{opt}, \tilde{\xi}^{[2]}_{g,opt}\right)$	$\left(\tilde{\omega}^{[2]}_{A}, \tilde{\omega}^{[2]}_{B}\right)$	$\tilde{h}^{[2]}_{FP}$	$\left(\tilde{v}^{[2]}_{FP}, \tilde{\xi}^{[2]}_{g,FP}\right)$
0.05	6.0486	(1.0267, 0.1420)	(0.9337, 1.0921)	6.0531	(1.0260, 0.1387)
0.10	4.0744	(1.0580, 0.2097)	(0.9154, 1.1378)	4.0876	(1.0541, 0.1987)
0.20	2.5645	(1.1477, 0.3360)	(0.9172, 1.2008)	2.6186	(1.1180, 0.2887)
0.30	-	-	-	1.9222	(1.1952, 0.3638)

where $Z_g = \zeta_g^2$. Similarly, the second resultant equation in (40) becomes

$$\tilde{R}^{[2]}_2(r) = \sum_{i=0}^{4} \tilde{\kappa}^{[2]}_i(\mu)\, r^i = 0, \tag{43}$$

in which $\tilde{\kappa}^{[2]}_i$ are coefficients in the mass ratio μ. Note from the forms of Eqs. (42) and (43) that no closed-form exact solution $\left(r^{[2]}_{\min}, \tilde{v}^{[2]}_{opt}, \tilde{\xi}^{[2]}_{g,opt}\right)$ exists even if the grounded damping is with the absorber and even if the approximate solution $\left(\tilde{v}^{[2]}_{FP}, \tilde{\xi}^{[2]}_{g,FP}\right)$ has a quite simple form. According to Theorem 1, the existence of feasible solutions $r \in (0,1)$ of the univariate polynomial Eq. (43) is necessary for an operable exact optimization. In particular, the coefficients $\tilde{\kappa}^{[2]}_i$ are

$$\begin{cases} \tilde{\kappa}^{[2]}_0 = 16\mu^2\left(\mu^4 - 5\mu^3 + 15\mu^2 - 5\mu + 1\right), \\ \tilde{\kappa}^{[2]}_1 = -16\mu\left(3\mu^4 - 14\mu^3 + 66\mu^2 - 21\mu + 4\right), \\ \tilde{\kappa}^{[2]}_2 = -4\left(8\mu^6 - 44\mu^5 + 133\mu^4 - 170\mu^3 - 287\mu^2 + 88\mu - 16\right), \\ \tilde{\kappa}^{[2]}_3 = 4\left(12\mu^5 - 54\mu^4 + 257\mu^3 - 457\mu^2 + 12\mu\right), \\ \tilde{\kappa}^{[2]}_4 = 16\mu^6 - 96\mu^5 + 300\mu^4 - 628\mu^3 + 469\mu^2 + 336\mu - 64. \end{cases} \tag{44}$$

Comparisons are twofold to demonstrate the benefits of the exact optimization and the grounded damping ζ_g.

4.2.1. *Comparisons with the fixed-point method*

Also taking μ as a variable, Eq. (43) depicts the implicit relationship between μ and r, as shown in Fig. 4(a). The meaningful intervals where $\mu > 0$ and $0 < r < 1$ are zoomed in Fig. 4(b), where a minimum of r labeled as r_{low} exists. Clearly, the value of μ should lie within the region where $r \geqslant r_{low}$ leading to $\mu \in (0, \mu_{up})$. Given the extremum condition $\partial r/\partial \mu = 0$ and the polynomial form of Eq. (43), we consider the resultant equation similar to Eq. (35)

$$\tilde{R}^{[2]}_3(r) = \mathcal{D}_\mu\left(\tilde{R}^{[2]}_2(\mu, r), \frac{\tilde{R}^{[2]}_2(\mu, r)}{\partial r}\right) = r^5(r+1)^7(r-1)^5 \sum_{i=0}^{27} \tilde{\rho}^{[2]}_i r^i = 0, \tag{45}$$

where $\tilde{\rho}^{[2]}_i$ are real constant coefficients. The minimum $r_{low} = 0.8416$ can be solved from Eq. (45) so that $\mu_{up} = 0.2813$ as per Eq. (43), both of which agree with Fig. 4. The exactly- and approximately- optimized AMF curves for four mass ratios $\mu = [0.05, 0.1, 0.2, 0.3]$ are compared in Fig. 5, and the associated parameters are detailed in Table 2.

The solid curves in Fig. 5 represent the EO-AMF, and the observed two equal peaks again verify the proposed exact optimization procedure. The two resonance frequencies $\left(\tilde{\omega}^{[2]}_A, \tilde{\omega}^{[2]}_B\right)$ in Table 2 are calculated following Lemma 4 and agree with Fig. 5. The

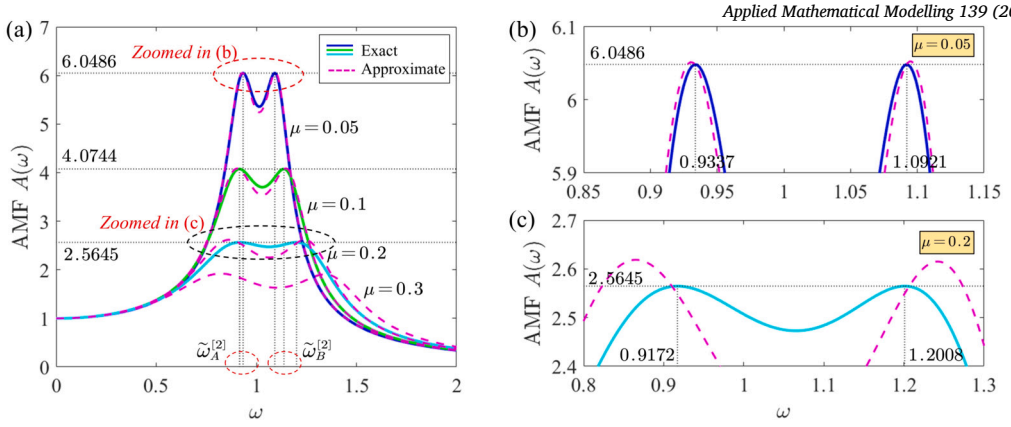

Fig. 5. (a). Comparisons between the exactly- (solid) and approximately- (dashed) optimized AMF curves. (b) and (c) are zoomed plots of (a) for $\mu=0.05$ and $\mu=0.2$, respectively.

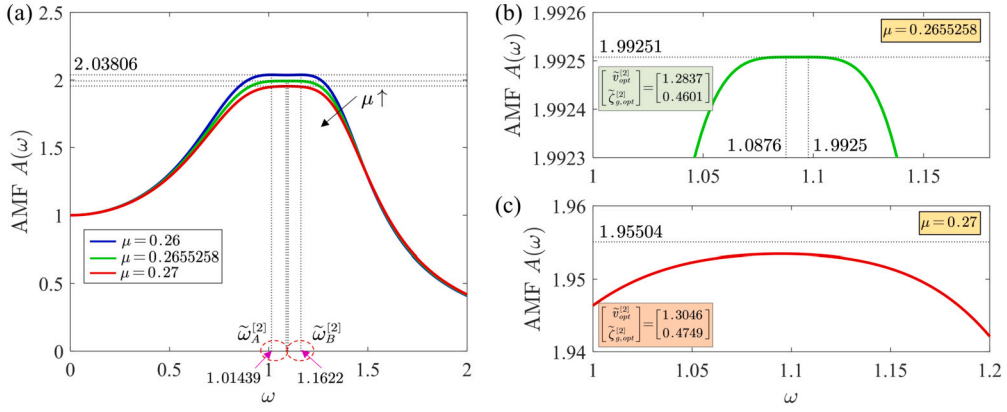

Fig. 6. (a). EO-AMF curves for $\mu=[0.26, 0.2655258, 0.27]$. (b) and (c) are zoomed plots of (a) for $\mu=0.2655258$ and $\mu=0.27$, respectively.

parameter $\tilde{h}_{FP}^{[2]}$ in Table 2 represents the maximum of the AMF optimized by the fixed-point method with $\left(\tilde{v}_{FP}^{[2]}, \tilde{\zeta}_{g,FP}^{[2]}\right)$. From Fig. 5, the approximately optimized AMFs are close to the EO-AMFs for a small μ, and the accuracies of the fixed-point method decrease as μ increases. Meanwhile, the optimized peaks $\left(\tilde{h}_{\min}^{[2]}, \tilde{h}_{FP}^{[2]}\right)$ reduce with μ, and obviously, the DVA tuned with the exact optimum pair of $\left(\tilde{v}_{FP}^{[2]}, \tilde{\zeta}_{g,FP}^{[2]}\right)$ always renders a beneficially lower AMF peak height (i.e., $\tilde{h}_{\min}^{[2]} < \tilde{h}_{FP}^{[2]}$). Note from Fig. 4(b) that no solutions r of Eq. (43) exist when $\mu > \mu_{up} = 0.2813$, and it is verified in Fig. 5(a) and Table 2, where the exact H_∞ optimization problem remains unsolved for $\mu = 0.3$. This example shows that the cases where the fixed-point method is applicable do not mean that the exact optimization is operable.

To investigate the absence of exact solutions when $\mu > \mu_{up}$, we consider three cases $\mu = [0.26, 0.2655258, 0.27]$, in which $\mu = 0.2655258$ is the exact upper bound for operable exact optimization and is obtained by dense numerical sweeping of μ. The corresponding EO-AMF curves and the related key parameters are incorporated in Fig. 6.

From Fig. 6(a), the exact optimization for $\mu = 0.26$ results in two equal peaks, and the according resonance frequencies agree with Lemma 4 as expected. When increasing to $\mu = 0.2655258$, the associated EO-AMF curve is zoomed in Fig. 6(b), which is the critical moment when the two resonance peaks and the antiresonance peak are of the same height. In this case, the theoretical minimum peak as per (15), i.e., $\tilde{h}_{\min}^{[2]} = 1.99251$, and the two resonance frequencies as per Lemma 4 still well predict system responses. However, when further increasing to $\mu = 0.27 < \mu_{up}$, as zoomed in Fig. 6(c), the theoretical prediction $\tilde{h}_{\min}^{[2]} = 1.95504$ fails since the AMF only exhibits a single peak, agreeing with Fig. 5. This observation verifies Lemma 3 and the necessary condition provided by Theorem 1. Clearly, with Theorem 1, one can now analytically locate near the exact upper bound before numerical sweeping to reduce computational costs, another advantage of the proposed resultant-based procedure, in addition to the simplified nonconservative solving process.

The exactly optimized compositions $\left(\tilde{h}_{\min}^{[2]}, \tilde{v}_{opt}^{[2]}, \tilde{\zeta}_{g,opt}^{[2]}\right)$ and the approximate ones $\left(\tilde{h}_{FP}^{[2]}, \tilde{v}_{FP}^{[2]}, \tilde{\zeta}_{g,FP}^{[2]}\right)$ via the fixed-point method with sweeping $\mu \in [0.05, 0.5]$ are compared in Fig. 7. From Fig. 7(a), exact solutions if exist always yield a smaller maximum peak height $\tilde{h}_{\min}^{[2]}$ than the approximate one $\tilde{h}_{FP}^{[2]}$, and the differences between such two increase as μ grows, a direct result of the enlarged difference between $\left(\tilde{v}_{opt}^{[2]}, \tilde{\zeta}_{g,opt}^{[2]}\right)$ and $\left(\tilde{v}_{FP}^{[2]}, \tilde{\zeta}_{g,FP}^{[2]}\right)$, as shown in Fig. 7(b) and (c). Furthermore, the newly obtained upper bound $\mu = 0.2655 < \mu_{up}$ for the operable exact optimization concurs with Fig. 4(b) and Fig. 6. The differences in optimization operability

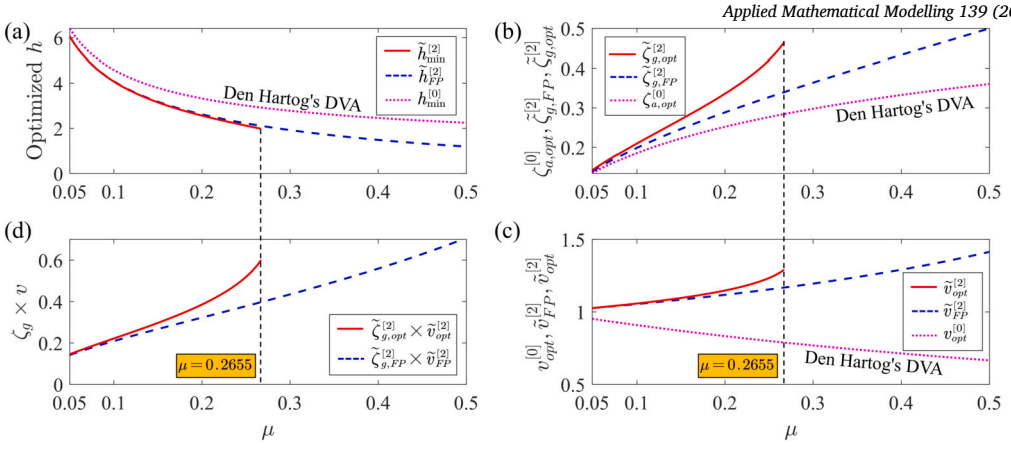

Fig. 7. (a). $\left(h_{\min}^{[0]}, \tilde{h}_{FP}^{[2]}, \tilde{h}_{\min}^{[2]}\right)$ versus μ. (b). $\left(v_{opt}^{[0]}, \tilde{v}_{FP}^{[2]}, \tilde{v}_{opt}^{[2]}\right)$ versus μ. (c). $\left(\zeta_{a,opt}^{[0]}, \tilde{\zeta}_{g,FP}^{[2]}, \tilde{\zeta}_{g,opt}^{[2]}\right)$ versus μ. Den Hartog's DVA in (a, b, d) refers to Fig. 1(b). (d). An indirect reflection of the variations of the optimized $\bar{c}_g$ given $\bar{c}_g = 2\bar{m}_a\bar{\omega}_a\zeta_g$.

in the exact and approximate cases indicate that the AMF has different sensitivities to such two cases, even though the resulting optimized peak height h does not differ much in two cases. To this end, Theorem 1 helps guide the design of a DVA that can be exactly optimized or customize the selection of the optimization method to be used. At last, Fig. 7(d) reflects the variations of $\bar{c}_g$ in light of $\bar{c}_g = 2\bar{m}_a\bar{\omega}_a\zeta_g$. Combining with Fig. 6(b) and Fig. 7(c, d), one can find that a single peak appears when $\left(\bar{c}_g, \bar{k}_a\right)$ are large for a given μ or $\bar{m}_a$, see also Remark 1.

4.2.2. Comparisons with Den Hartog's DVA

Note that the only difference between the DVA considered here with $\left(\zeta_p = \zeta_a = 0, \zeta_g > 0\right)$ and the classic Den Hartog's DVA shown in Fig. 1(b) is the position of the absorber damper. The damper of the present DVA is connected to the ground, while that of Den Hartog's DVA is connected to the primary structure (i.e., $\zeta_a > 0, \zeta_g = \zeta_p = 0$). The exactly optimized parameter pair $\left(v, \zeta_a\right)$ of Den Hartog's DVA is explicitly given in [41], which is denoted as

$$\begin{cases} v_{opt}^{[0]} = \dfrac{2}{1+\mu}\sqrt{\dfrac{2\left[2(\mu+2)\sqrt{3\mu+4}+9\mu^2+23\mu+16\right]}{3\left(27\mu^2+80\mu+64\right)}}, \\ \zeta_{a,opt}^{[0]} = \dfrac{1}{4}\sqrt{\dfrac{8+9\mu-4\sqrt{4+3\mu}}{\mu+1}}. \end{cases} \tag{46}$$

Accordingly, the peak height of the EO-AMF associated with Den Hartog's DVA is labeled as $h_{\min}^{[0]}$. The optimized parameter composition $\left(h_{\min}^{[0]}, v_{opt}^{[0]}, \zeta_{a,opt}^{[0]}\right)$ is superposed as the magenta dotted curves in Fig. 7. From Fig. 7(a), the optimized DVA with grounded damping ζ_g outperforms that with the damping ζ_a between the absorber and primary structure, as featured in the relationship of $\tilde{h}_{\min}^{[2]} < \tilde{h}_{FP}^{[2]} < h_{\min}^{[0]}$, agreeing with results in [5]. On the other hand, the optimized parameter pairs are compared in Fig. 7(b) and (c), where the larger values of the pairs $\left(\tilde{\zeta}_{g,opt}^{[2]}, \tilde{\zeta}_{g,FP}^{[2]}\right)$ and $\left(\tilde{v}_{opt}^{[2]}, \tilde{v}_{FP}^{[2]}\right)$ than the associated values of $\left(v_{opt}^{[0]}, \zeta_{a,opt}^{[0]}\right)$ mean that the optimized DVA with grounded damping ζ_g exhibits harder dynamical characteristics (i.e., larger stiffness $\bar{k}_a$ and damping $\bar{c}_a$), yielding a more compact DVA working space. Such benefits are more apparent as the mass ratio μ or equivalently the absorber mass $\bar{m}_a$ increases. Hence, connecting the DVA damper to the ground, if applicable, is recommended for protecting both the primary structure and the DVA. The combined effects of ζ_a and ζ_g are evaluated next.

4.3. Optimization when $\zeta_a > 0$

No approximate solutions exist when the two damping ζ_a and ζ_g take effect simultaneously. The optimization is twofold to benefit demonstration. We first optimize ζ_g for a given ζ_a, then we consider the reversed case for the optimal ζ_a. Proceeding from Fig. 5, the EO-AMF by optimizing $\left(v, \zeta_g\right)$ for $\mu = [0.1, 0.2]$ and several ζ_a values are shown in Fig. 8(a).

Once ζ_a is effective, Eqs. (39) and (40) are used for optimizing $\left(v, \zeta_g\right)$, and accordingly, the optimized parameters are denoted as $\left(v_{opt}^{[2]}, \zeta_{g,opt}^{[2]}\right)$. From Fig. 8(a), increasing ζ_a unfavorably raises the optimized peak heights regardless of μ, again showing that putting more weights on the grounded damping ζ_g benefits DVA performance. To further clarify this, we optimize ζ_a with sweeping ζ_g following a procedure similar to Fig. 2, leading to Fig. 8(b) and (c), where the solid magenta curves are with $\zeta_g = 0$ representing the EO-AMF corresponding to Den Hartog's DVA, and the blues ones concur with those in Fig. 8(a).

From Fig. 8(b) and (c), the EO-AMF exhibits lower peaks as ζ_g increases by converging to the reduced case with $\zeta_a = 0$, and then no solutions exist once $\zeta_g > \tilde{\zeta}_{g,opt}^{[2]}$. Hence, an additional energy-consuming component does not necessarily mean an improvement in the

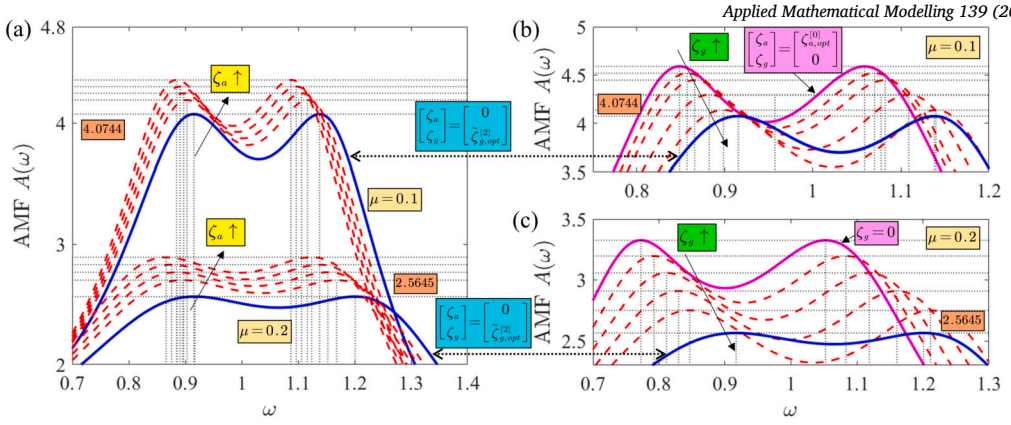

Fig. 8. (a). EO-AMF with $\left(v^{[2]}_{opt},\zeta^{[2]}_{g,opt}\right)$ for $\zeta_a=[0,0.04,0.06,0.08,0.1]$. The solid blue two are with $\zeta_a=0$. (b-c). EO-AMF with $\left(v^{[2]}_{opt},\zeta^{[2]}_{a,opt}\right)$ for given values of ζ_g. The solid magenta and blue ones are with $\zeta_g=0$ and $\zeta_a=0$, respectively.

vibration suppression performance from the perspective of H_∞ optimization. This counter-intuitive observation provides guidance for the practical optimal DVA design, which is to reduce the damping ζ_a between the DVA and the primary structure, and in the meantime, increase DVA's grounded damping ζ_g as much as possible. Note, however, that possible constraints for this in engineering practice might be the difficulty in attaching the DVA components to the ground.

On the other hand, the results in Fig. 8(a-c) imply that no parameter composition (v,ζ_a,ζ_g) exists to simultaneously satisfy the two extremum conditions $\partial r/\partial\zeta_a=0$ and $\partial r/\partial\zeta_g=0$ since the peak heights of the EO-AMFs vary monotonously with respect to ζ_a and ζ_g until no exact solutions exist. That is, no analytical solving procedure can directly yield the exact optimal composition of (v,ζ_a,ζ_g) or the associated EO-AMF, and a feasible calculating procedure for this is to optimize one of the two damping (ζ_a,ζ_g) by sweeping the other one as in Fig. 8. Clearly, the given results show that optimizing ζ_g with a fixed $\zeta_a=0$ leads to the best DVA performance for lower EO-AMF peak heights.

5. Case 3: grounded damping in both primary structure and DVA $(\zeta_p>0,\zeta_g>0)$

Both grounded dampings ζ_p and ζ_g are now activated, and the associated optimized DVA is compared to those in Fig. 1(b-e). Since introducing ζ_a partially neutralizes the benefits of ζ_g as per Section 4.3, we optimize (v,ζ_g) while fixing $\zeta_a=0$. The optimization can still be directly generalized from Fig. 2, in which the equations to be handled are updated as follows.

5.1. Equations to be handled

With $(\zeta_p>0,\zeta_g>0,\zeta_a=0)$, Eq. (14) can be separated into two polynomial equations in ζ_g in the forms of

$$\begin{cases} f^{[3]}_{1,[r,v]}(\zeta_g)=\sum_{i=0}^{2}\alpha^{[3]}_i(r,v)\,\zeta_g^i=0,\\ f^{[3]}_{2,[r,v]}(\zeta_g)=\sum_{i=0}^{4}\beta^{[3]}_i(r,v)\,\zeta_g^i=0,\end{cases} \tag{47}$$

where $\alpha^{[3]}_i$ and $\beta^{[3]}_i$ are polynomial coefficients in (r,v), and $\max\left\{deg\left[\alpha^{[3]}_i,v\right]\right\}=\max\left\{deg\left[\beta^{[3]}_i,v\right]\right\}=4$. Substituting Eq. (47) into the associated equations in Fig. 2 and selecting $(\vartheta,i)=(g,3)$, the two intermediate resultant equations take the updated forms of

$$\begin{cases} R^{[3]}_1(r,V)=simplify\left(\mathcal{D}_{\zeta_g}\left(f^{[3]}_1,f^{[3]}_2\right)\right)=\sum_{i=0}^{10}\gamma^{[3]}_i(r)\,V^i=0,\\ R^{[3]}_2(r)=simplify\left(\mathcal{D}_V\left(R^{[3]}_1,\frac{\partial R^{[3]}_1}{\partial V}\right)\right)=\sum_{i=0}^{62}\kappa^{[3]}_i r^i=0,\end{cases} \tag{48}$$

where $\gamma^{[3]}_i$ are coefficients in r, $\kappa^{[3]}_i$ are real constants, and the function $simplify(\cdot)$ is consistent with that in Eqs. (40). The obtained optimum parameter composition for a given ζ_p is denoted as $\left(r^{[3]}_{\min},v^{[3]}_{opt},\zeta^{[3]}_{g,opt}\right)$.

5.2. Comparisons with existing DVAs

Selecting $\mu=0.05$, the resulting EO-AMF curves for $\zeta_p=0$ and $\zeta_p=0.1$ are respectively shown as the solid red and cyan curves in Fig. 9(a), where the equal-peak features and the resonance frequencies again verify the presented theoretical analysis. Besides, with the same μ and with the grounded stiffness removed to streamline with the condition $\eta=0$ of Section 2, the optimized AMF associated with the classic DVA by Den Hartog [2], the lever-type DVA by Shen et al. [30], and the flywheel-type DVA by Baduidana et al. [31] are also superposed for comparisons. In particular, Den Hartog's DVA is exactly optimized by Eq. (46), and Shen's and Baduidana's DVAs are optimized by the fixed-point method following the associated references, with

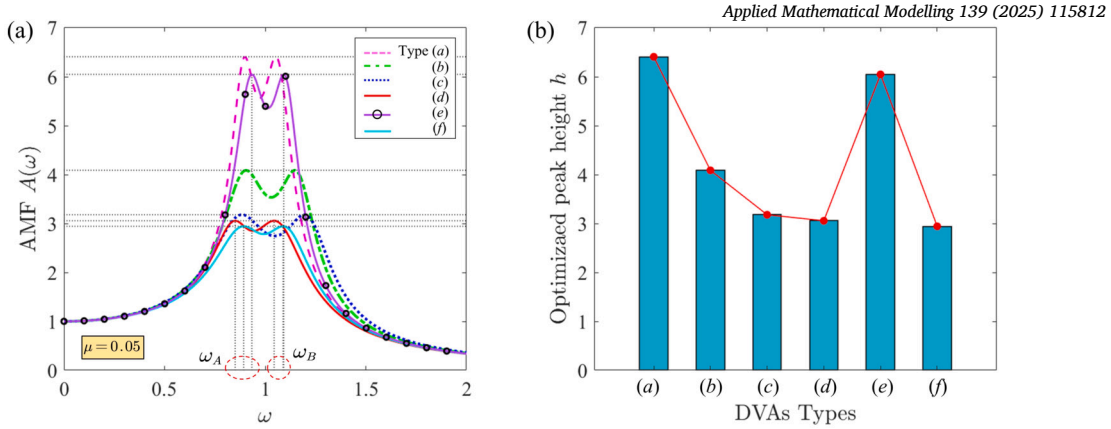

Fig. 9. (a). Comparisons of optimized AMFs for various DVAs listed in Table 3. (b). The peak values of the AMF curves in (a).

Table 3
Parameters associated with Fig. 9(a).

DVAs	ζ_p	L_1 or L_2	Optimized parameters	h
Den Hartog (*a*)	0	-	$\left(\upsilon_{opt}^{[0]}, \zeta_{a,FP}^{[0]}\right) = (0.9524, 0.1339)$	6.4079
Shen's (*b*)	0	$\sqrt{2}$	$\left(\upsilon_{FP}^{[L]}, \zeta_{g,FP}^{[L]}\right) = (1.0615, 0.2214)$	4.0875
Baduidana's (*c*))	0	$\sqrt{2}$	$\left(\upsilon_{FP}^{[F]}, \zeta_{g,FP}^{[F]}\right) = (1.8787, 0.2136)$	3.1796
DVA in Case 1 (*d*)	0.1	-	$\left(\upsilon_{opt}^{[1]}, \zeta_{a,opt}^{[1]}\right) = (0.9138, 0.1476)$	3.0567
DVA in Case 2 (*e*)	0	-	$\left(\tilde{\upsilon}_{opt}^{[2]}, \tilde{\zeta}_{g,opt}^{[2]}\right) = (1.0267, 0.1420)$	6.0486
DVA in Case 3 (*f*)	0.1	-	$\left(\upsilon_{opt}^{[3]}, \zeta_{g,opt}^{[3]}\right) = (1.0021, 0.1615)$	2.9435

$$\begin{cases} \upsilon_{FP}^{[L]} = \sqrt{\dfrac{1}{1-L_1^2\mu}}, \\ \zeta_{a,FP}^{[L]} = \sqrt{\dfrac{3L_1^2\mu}{8-4L_1^2\mu}}, \end{cases} \quad \begin{cases} \upsilon_{FP}^{[F]} = \sqrt{\dfrac{1+L_2^2}{1-\mu\left(1+L_2^2\right)}}, \\ \zeta_{g,FP}^{[F]} = \sqrt{\dfrac{3\mu\left(1+L_2^2\right)^2}{4L_2^4\left[2-\mu\left(1+L_2^2\right)\right]}}, \end{cases} \tag{49}$$

where the two superscripts $(\cdot)^{[L]}$ and $(\cdot)^{[F]}$ denote the lever- and flywheel-type DVAs, respectively, $L_1 = \bar{l}_1/\bar{l}_2$ and $L_2 = \bar{r}_1/\bar{r}_2$ are amplification ratios, see Fig. 1 for the definitions of the four lengths $\left(\bar{l}_1, \bar{l}_2, \bar{r}_1, \bar{r}_2\right)$. Note from the form of Eq. (49) that such structural modifications into the DVA function as effects of an inerter to alter DVA's equivalent proof mass (i.e., μ is amplified), as aforementioned. With $L_1 = L_2 = \sqrt{2}$, the parameters and peak heights associated with Fig. 9(a) are detailed in Fig. 9(b) and Table 3, respectively.

From Fig. 9(a) and (b), the peak height of the optimized AMF corresponding to the classic Den Hartog's DVA is sequentially reduced by modifying its construction to Shen's (*b*) and then Baduidana's (*c*) DVAs, thus enhancing the vibration suppression performance. In comparison, the optimized DVA in Case 1 with $\left(\zeta_a > 0, \zeta_g = 0\right)$ is also considered, leading to the EO-AMF denoted by (*d*). The lower peak height of the AMF (*d*) than those of the two (*b*) and (*c*) reveals the strength of the damping ζ_p of the primary structure in vibration suppression. That is, by injecting slight damping into the primary structure, further enhanced vibration suppression performance can be achieved without the need for structural modifications in DVA. Note also that Shen's (*b*) and Baduidana's (*c*) DVAs require an additional fulcrum for installing the lever and the flywheel, which, however, can be inaccessible in practice. On the other hand, suppressing the peak height by unduly raising the two amplification ratios L_1 and L_2 requires architectural space and can lead to fractures and failures on the fulcrum, and a similar conclusion holds if we directly adopt the inerter component. Hence, optimizing a DVA with ignoring the damping ζ_p of the primary structure or assuming that ζ_p is small can lead to conservative results for both the optimization method and the optimized vibration suppression performance. Furthermore, the damping ζ_p can also enhance the DVA performance in Case 2 so that the EO-AMF is suppressed from (*e*) to (*f*), the peak height of which is the lowest among the shown cases yielding the best performance.

6. Algorithm details and experimental comparisons for computational efficiency

More details on the implementation of the Dixon resultant-based exact optimization procedure proposed in Fig. 2 are introduced in this section. Moreover, we demonstrate the improved computational efficiency of the Dixon resultant compared with the previously adopted Syvester's one in [48–50,52], as well as the computational benefits of such a univariate-polynomial-equation-based procedure over Nishihara's numerical method [37].

Table 4
Average computational costs of applying Dixon and Sylvester resultants for the results of Fig. 3(a).

	Constructing $R_1^{[1]}(r,V)$			Constructing $R_2^{[1]}(r)$		
	Dimension of **S** or **D**	Memory used	CPU time used	Dimension of **S** or **D**	Memory used	CPU time used
Sylvester-type	6×6	277.3 KiB	<1 ns	15×15	197.76 MiB	0.507 s
Dixon-type	4×4	19.32 KiB	<1 ns	8×8	9.64 MiB	<1 ns

Table 5
Average computational costs of Dixon and Sylvester resultants for the results of Fig. 8(a-c) with $\zeta_a, \zeta_g > 0$.

	Constructing $R_1^{[2]}(r,V)$			Constructing $R_2^{[2]}(r)$		
	Dimension of **S** or **D**	Memory used	CPU time used	Dimension of **S** or **D**	Memory used	CPU time used
Sylvester-type	6×6	500.76 KiB	<1 ns	23×23	437.29 MiB	0.903 s
Dixon-type	4×4	17.12 KiB	<1 ns	12×12	195.80 MiB	0.172 s

Table 6
Average computational costs of Dixon and Sylvester resultants for the EO-AMF (f) in Fig. 9 with $\zeta_p, \zeta_g > 0$.

	Constructing $R_1^{[3]}(r,V)$			Constructing $R_2^{[3]}(r)$		
	Dimension of **S** or **D**	Memory used	CPU time used	Dimension of **S** or **D**	Memory used	CPU time used
Sylvester-type	6×6	238.09 KiB	<1 ns	19×19	337.65 MiB	0.544 s
Dixon-type	4×4	15.02 KiB	<1 ns	10×10	11.76 MiB	0.016 s

All computational works are performed on a standard laptop with a 2.2 GHz 13th Gen Intel i9-13900HX CPU and 16 GB RAM, and MAPLE 2023 and MATLAB 2023a are used as software platforms. In addition, no elaborate codes and toolboxes are used to benefit comparisons.

6.1. Comparisons between Dixon and Sylvester resultants

Revisiting Fig. 2, the resultant operation is deployed twice to trigger the solving process, i.e., the polynomial $R_2^{[i]}(r)$, $i=1,2,3$. The excluded factors of each polynomial equation corresponding to inappropriate solutions with $r \notin (0,1)$ and $V<0$ are determined using the command **gcd** (greatest common divisor of polynomials), which is well embedded in both MAPLE and MATLAB. Replacing the Dixon matrix in the constructing process with Syvester's one results in a Syvester resultant-based optimization procedure. Comparisons in light of [53] are given to show the strength of the newly introduced Dixon matrix.

With MAPLE, the average computational costs in the constructing process for the three Cases given in Sections 3, 4, and 5 are compared in Tables 4, 5, and 6, respectively, where the costs of memory and CPU time are measured by the built-in command **Usage**, and all variables except for the ones to be optimized are numerically evaluated before operations to reduce symbolic calculations. The benefits of Dixon resultant are apparent from Tables 4, 5, and 6, where the memory and CPU time used for constructing $R_2^{[i]}(r)$, $i=1,2,3$ by Dixon matrix are respectively decreased by more than 50% and 80% compared with those based on Sylvester matrix. Clearly, such benefits can be more obvious if the EO-AMF corresponding to multiple parameter compositions are required, exemplified by the optimizing produce discussed in Fig. 8. On the other hand, the computational costs are highly related to the matrix dimension, which is further related to the number of the resultant operations. Hence, the Sylvester resultant-based calculations may crash or halt in more involved cases, for instance, the three-element DVA given in [42], considering that three parameters of this DVA can be optimized for the EO-AMF, and thus a minimum of three resultant operations is required.

6.2. Comparisons between different solving procedures

As mentioned in Section 2.3 and demonstrated in Fig. 2, the given resultant-based optimization procedure is non-conservative to complement Nishihara's method [37]. Having established the univariate polynomial equations to be handled in Section 6.1, we compare the computational costs of such two methods in the solving process using MATLAB.

No closed-form solutions exist if either one of the grounded damping ζ_g or ζ_p is introduced. To this end, Nishihara's method simultaneously solves three ternary equations, i.e., the two in Eq. (14) plus the one resulting from the Jacobian matrix (19). The command **vpasolve**, which can exhaustively detect solutions of a set of polynomial equations within a given range, is used to guarantee the global minimum condition. Besides, if given an initial guess, such as the pair $\left(\upsilon_{opt}^{[0]}, \zeta_{a,opt}^{[0]}\right)$ in (46) for the optimization in Case 1 as in [37], the command **fsolve** that finds the solution nearest to the initial guess is available for Nishihara's method, and clearly, in this case, a proper initial guess is critical for the global minimum condition.

Since the solving steps of Fig. 2 handle purely univariate polynomial equations, the more concise command **roots**, which routinely calculates the standard QR decomposition and companion matrix [59], can be deployed instead for higher efficiency. In the test, $\left(\upsilon_{opt}^{[0]}, \zeta_{a,opt}^{[0]}\right)$ is used as the initial guess for the optimization in Case 1, the approximate solution $\left(\upsilon_{FP}^{[L]}, \zeta_{g,FP}^{[L]}\right)$ with $L_1=1$ given

Table 7
Average computational time cost when using different solving methods. 'NIG' and 'GIG' mean "No initial guesses" and "Given initial guesses", respectively.

Cases	Nishihara's method (**vpasolve**, NIG)	Nishihara's method (**fsolve**, GIG)	Our method (**roots**, NIG)	Our method (**fsolve**, GIG)
Case 1	5.858 s	0.153 s	0.171 s	0.044 s
Case 2 $(\zeta_a \neq 0)$	No solutions	0.214 s	0.483 s	0.087 s
Case 3 (EO-AMF (f) in Fig. 9(a))	24.342 s	0.177 s	0.191 s	0.053 s

in (49) is used for Cases 2 and 3, and the initial guess of r is consistently set as $r = 0.9$. The resulting time costs of the mentioned calculating methods, measured by the embedded command pair **tic** − **toc**, are compared in Table 7.

From Table 7, the efficiency of our resultant-based method is apparent when no initial guesses (NIG) are given. Although its time cost, in comparison, is slightly increased if Nishihara's method is given initial guesses (GIG), the time-cost magnitudes of these two methods are at the same level. Furthermore, once our resultant-based method receives an initial guess for each univariate polynomial equation, the resulting time cost can be suppressed to less than 0.1 s, the shortest among the shown cases. Note that getting a proper initial guess is not easy as the DVA construction varies or becomes more complex, and therefore, our resultant-based method, which guarantees the conditions for global optimum and convergence with no need for initial guesses, provides a robust solution for the exact H_∞ optimization. This feature is also the basis of generalizing this resultant-based procedure from the reduced Case 1 to Cases 2 and 3 and then to more involved optimization models.

Remark 7. Our exact resultant-based optimization procedure requires that the equations to be handled are polynomial, e.g., Eqs. (27), (39), and (47). The required sufficiently low computational costs shown above compensate for the possible concerns that the exact solutions are of non-closed forms while limitedly improving the DVA performance compared with the results of the fixed-point method. Besides, our method can handle the cases where the damping in the primary structure cannot be ignored. However, such conclusions do not mean that exact solutions should always be pursued given that they may not exist (see Fig. 7) or are hard to have (when $\eta \neq 0$). The core of our method in addition to the high efficiency and non-conservativeness is the characterization of the behaviors of exact solutions so that one can customize the optimization methods for different DVA variants. □

7. Remarks on the exact optimization when $\eta \neq 0$

As mentioned, all exact optimizations in this work are based on the condition $\eta = 0$ so that polynomial equations can be constructed for simplification. Some further considerations are given for the exact optimization problem when $\eta \neq 0$. Taking η into account and considering that ζ_a dilutes the benefits of ζ_g as per Section 4.3, we have three parameters (v, ζ_g, η) to be optimized. In this case, Lemma 2 cannot be used, and the equal-peak conditions for numerical exact optimization are

$$\begin{cases} \frac{\partial A(\omega, v, \zeta_g, \eta)}{\partial \omega} |_{\omega=\omega_A} = 0, \\ \frac{\partial A(\omega, v, \zeta_g, \eta)}{\partial \omega} |_{\omega=\omega_B} = 0, \\ A(\omega_A, v, \zeta_g, \eta) - A(\omega_B, v, \zeta_g, \eta) = 0, \end{cases} \tag{50}$$

where ω_A and ω_B are the two resonance frequencies. Furthermore, the minimum condition of the peak height leads to

$$\begin{cases} \frac{\partial h(\omega, v, \zeta_g, \eta)}{\partial v} |_{\omega=\omega_A=\omega_B} = 0, or \\ \frac{\partial h(\omega, v, \zeta_g, \eta)}{\partial \zeta_g} |_{\omega=\omega_A=\omega_B} = 0, or \\ \frac{\partial h(\omega, v, \zeta_g, \eta)}{\partial \eta} |_{\omega=\omega_A=\omega_B} = 0, \end{cases} \tag{51}$$

or all three equations in (51) hold. Consequently, five unknowns $(\omega_A, \omega_B, v, \zeta_g, \eta)$ are governed by three equations (Eq. (50)) at least and six equations (Eqs. (50) and (51)) at most, leading to a non-convex optimization problem. The main difficulty is that the form of h, which depicts the maximum of the AMF as defined in (10), is unclear and is related to the composition (v, ζ_g, η). When $\zeta_p = \zeta_a = 0$, the fixed-point method yields approximate solutions. To avoid brute-force sweeping procedures for the exact optimization problem governed by Eqs. (50) and (51) regardless of the values of (ζ_p, ζ_a), more delicate calculation tools and optimization procedures are required. On the other hand, one may expect better DVA performance in the case with negative grounded stiffness $\eta < 0$, e.g., [30,31], which, however, requires specific mechanical design in practical realization [60]. That is, taking η or its equivalence as a constant coefficient of displacement can be inappropriate, which further complicates the optimization. All the above issues deserve to be further investigated in future work.

8. Conclusions

Based on a general 2DOF vibration absorption system, we investigate the parametric effects on the less-reported operability of the exact H_∞ optimization and on the vibration suppression to achieve the optimal DVA design. Accordingly, a Dixon resultant-based optimization procedure is proposed to complement Nishihara's numerical method and the widely adopted approximate fixed-point method, aiming to establish a non-conservative, efficient, easy-to-implement, and systematic framework for DVA optimization. The main results are as follows.

1). For optimization operability:

- Numerical procedures are the only solution for the exact H_∞ optimization if the DVA has a grounded stiffness with $\eta \neq 0$, regardless of the values of the damping ζ_p of the primary structure.
- By exclusively constructing and solving univariate polynomial equations, a necessary condition for the operably exact optimization is established in Theorem 1. This benefits the design of an exactly optimizable DVA or customizes the selection of the optimization methods to be used, thus maximizing the vibration suppression performance.
- Applying Dixon resultant rather than Sylvester's can reduce computational time by more than 80%, and such benefits can be more apparent as the DVA configuration or system dynamics become more complex.
- If the primary structure is damped (i.e., $\zeta_p > 0$) as in Case 1, the AMF curve exhibiting two peaks of an identical height may be locally optimum. Thus, numerical optimization only based on the equal-peak condition can be conservative.
- If the DVA has a grounded damping ζ_g as in Case 2, exact optimization may only be operable in a certain range, which can be checked by Theorem 1. Moreover, an optimization that can be handled by the fixed-point method does not necessarily lead to exact solutions. Besides, no analytical conditions exist to simultaneously optimize the three $(\upsilon, \zeta_a, \zeta_g)$.

2). For the optimum vibration suppression performance:

- Damping ζ_a between the DVA and the primary structure compromises the benefits of the grounded damping ζ_g, indicating that an additional energy-consuming component does not always improve DVA performance. Thus, optimizing ζ_g while reducing ζ_a is recommended.
- Damping ζ_p in the primary structure is beneficial in enhancing vibration suppression as per Case 3. With a small ζ_p injected into the classic Den Hartog's DVA, the EO-AMF peak height associated with the resulting DVA in (*c*) can be further reduced as compared with that associated with the DVAs based on structural modifications, e.g., Fig. 1(d) and (e). Furthermore, damping ζ_p can take effect jointly with ζ_g to further lower the EO-AMF peak height. Hence, letting $\zeta_p = 0$ as in Fig. 1(b), (d), and (e) can lead to conservative results for both vibration suppression and DVA optimization.

We stress that the results reached above can apply to a large range of DVA variants with various structural modifications or component arrangements as long as such operations are equivalent to the tuning of $(\bar{m}_a, \bar{c}_a, \bar{k}_a, \bar{c}_g, \bar{c}_p)$, exemplified by Eq. (49) for tuning $\bar{m}_a$ via the link length $(\bar{l}_1, \bar{l}_2)$. Similarly, the resultant-based procedure in Fig. 2, with high efficiency and non-conservativeness, can be generalized to various polynomial-equations-based optimization problems including the MDOF DVAs in [38–40]. The authors believe that this work enriches the state-of-the-art knowledge of the H_∞ optimization problem and provides a benchmark theory for exact optimization. Issues mentioned in Section 7 and optimization combined with modal analysis as in [8–10] will be our next stage of work.

CRediT authorship contribution statement

Yifan Liu: Writing – review & editing, Writing – original draft, Conceptualization. **Li Cheng:** Writing – review & editing, Supervision, Resources, Project administration, Conceptualization.

Declaration of competing interest

The authors declare that they have no known competing financial interests or personal relationships that could have appeared to influence the work reported in this paper.

Appendix A. A simple comparison between Dixon and Sylvester matrix

Following [56], we consider two polynomial equations parameterized in λ with $d_1 = deg\left[p_1(\lambda), \lambda\right] = 1$ and $d_2 = deg\left[p_2(\lambda), \lambda\right] = 2$ so that $d_{\max} = \max\left\{d_1, d_2\right\} = 2$,

$$\begin{cases} p_1(\lambda) = \alpha_0 + \alpha_1 \lambda, \\ p_2(\lambda) = \beta_0 + \beta_1 \lambda + \beta_2 \lambda^2. \end{cases} \tag{52}$$

Then, the Dixon polynomial is constructed following (28) as

$$\delta(\lambda,\wp)=\frac{1}{\lambda-\wp}\begin{vmatrix}\alpha_0+\alpha_1\lambda & \beta_0+\beta_1\lambda+\beta_2\lambda^2\\ \alpha_0+\alpha_1\wp & \beta_0+\beta_1\wp+\beta_2\wp^2\end{vmatrix}=\left(-\alpha_1\beta_2\lambda-\alpha_0\beta_2\right)\wp+\left(-\alpha_0\beta_2\lambda-\alpha_0\beta_1+\alpha_1\beta_0\right). \tag{53}$$

Note that $deg\left[\delta(\lambda,\wp),\wp\right]=d_{\max}-1$ and each common solution λ of Eq. (52) is a zero of $\delta(\lambda,\wp)=0$ regardless of $\wp$. Hence, all the coefficients of $\wp$ should vanish at each common solution of Eq. (52), leading to the Dixon matrix

$$\mathbf{D}=\begin{bmatrix}-\alpha_0\beta_2 & -\alpha_1\beta_2\\ -\alpha_0\beta_1+\alpha_1\beta_0 & -\alpha_0\beta_2\end{bmatrix} \tag{54}$$

which is independent of λ and has the dimension of $d_{\max}\times d_{\max}$. The existence of any common solution of Eq. (52) requires

$$|\mathbf{D}|=\alpha_0^2\beta_2-\alpha_0\alpha_1\beta_1+\alpha_1^2\beta_0=0, \tag{55}$$

the so-called Dixon resultant equation. As for the Sylvester matrix [51,52] of Eq. (52), it is constructed as

$$\mathbf{S}=\begin{bmatrix}\alpha_1 & \alpha_0 & 0\\ 0 & \alpha_1 & \alpha_0\\ \beta_2 & \beta_1 & \beta_0\end{bmatrix}, \tag{56}$$

a matrix in the dimension of $\left(d_1+d_2\right)\times\left(d_1+d_2\right)$. Similarly, the Sylvester matrix $\mathbf{S}$ needs to be singular for the existence of any common solution of Eq. (52), yielding the Sylvester resultant equation

$$|\mathbf{S}|=\alpha_0^2\beta_2-\alpha_0\alpha_1\beta_1+\alpha_1^2\beta_0=0, \tag{57}$$

which is identical to (55). Clearly, the Dixon matrix (54) has a smaller dimension than that of the Sylvester matrix (56), and therefore the saved computational costs by applying the Dixon resultant can be substantial when any one of the two degrees d_1 and d_2 is large, as demonstrated in Section 6.1.

Data availability

Data will be made available on request.

References

[1] H. Frahm, Device for damping vibrations of bodies, 1911.
[2] J. Den Hartog, J. Ormondroyd, Theory of the dynamic vibration absorber, J. Appl. Mech. 50 (7) (1928) 11–22.
[3] J.E. Brock, A note on the damped vibration absorber, J. Appl. Mech. 13 (4) (1946) A284.
[4] J.P. Den Hartog, Mechanical Vibrations, Courier Corporation, 1985.
[5] M. Ren, A variant design of the dynamic vibration absorber, J. Sound Vib. 245 (4) (2001) 762–770.
[6] Y. Cheung, W.O. Wong, H-infinity optimization of a variant design of the dynamic vibration absorber—revisited and new results, J. Sound Vib. 330 (16) (2011) 3901–3912.
[7] W.O. Wong, Y. Cheung, Optimal design of a damped dynamic vibration absorber for vibration control of structure excited by ground motion, Eng. Struct. 30 (1) (2008) 282–286.
[8] S. Krenk, Frequency analysis of the tuned mass damper, J. Appl. Mech. 72 (6) (2005) 936–942.
[9] Y. Cheung, W.O. Wong, H∞ and h2 optimizations of a dynamic vibration absorber for suppressing vibrations in plates, J. Sound Vib. 320 (1–2) (2009) 29–42.
[10] H. Li, S. Wu, Q. Chen, Q. Fei, Design of dynamic absorbers to control the flexural resonant vibration of structures characterized by multiple natural modes, J. Sound Vib. 513 (2021) 116415.
[11] R. Sun, W. Wong, L. Cheng, Hybrid electromagnetic shunt damper with Coulomb friction and negative impedance converter, Int. J. Mech. Sci. 230 (2022) 107552.
[12] R. Sun, W. Wong, L. Cheng, Optimal design of a tunable electromagnetic shunt damper for dynamic vibration absorber, Mechatronics 83 (2022) 102763.
[13] R. Sun, W. Wong, L. Cheng, A tunable hybrid damper with Coulomb friction and electromagnetic shunt damping, J. Sound Vib. 524 (2022) 116778.
[14] Y. Shen, H. Peng, X. Li, S. Yang, Analytically optimal parameters of dynamic vibration absorber with negative stiffness, Mech. Syst. Signal Process. 85 (2017) 193–203.
[15] E. Barredo, A. Blanco, J. Colín, V.M. Penagos, A. Abúndez, L.G. Vela, V. Meza, R.H. Cruz, J. Mayén, Closed-form solutions for the optimal design of inerter-based dynamic vibration absorbers, Int. J. Mech. Sci. 144 (2018) 41–53.
[16] S. Chowdhury, A. Banerjee, The impacting vibration absorbers, Appl. Math. Model. 127 (2024) 454–505.
[17] S. Krenk, Resonant inerter based vibration absorbers on flexible structures, J. Franklin Inst. 356 (14) (2019) 7704–7730.
[18] R. Ma, K. Bi, H. Hao, Inerter-based structural vibration control: a state-of-the-art review, Eng. Struct. 243 (2021) 112655.
[19] A.d.S. Pippi, S.M. Avila, G. Doz, A review on the use of the inerter device in the structural coupling technique for adjacent building vibration control, Structures 42 (2022) 480–501.
[20] E. Barredo, G.L. Rojas, J. Mayén, A. Flores-Hernández, Innovative negative-stiffness inerter-based mechanical networks, Int. J. Mech. Sci. 205 (2021) 106597.
[21] S. Chowdhury, A. Banerjee, S. Adhikari, The optimal design of dynamic systems with negative stiffness inertial amplifier tuned mass dampers, Appl. Math. Model. 114 (2023) 694–721.
[22] J. Wang, Y. Zhang, D.T. Looi, Analytical h∞ and h2 optimization for negative-stiffness inerter-based systems, Int. J. Mech. Sci. 249 (2023) 108261.
[23] X. Wang, T. He, Y. Shen, Y. Shan, X. Liu, Parameters optimization and performance evaluation for the novel inerter-based dynamic vibration absorbers with negative stiffness, J. Sound Vib. 463 (2019) 114941.
[24] J. Deng, J. Zhao, J. Yang, Y. Tian, X. Long, Design and analysis of a tunable electromagnetic lever-type anti-resonant vibration isolator, Int. J. Mech. Sci. 263 (2024) 108787.
[25] C. Liu, X. Jing, F. Li, Vibration isolation using a hybrid lever-type isolation system with an x-shape supporting structure, Int. J. Mech. Sci. 98 (2015) 169–177.
[26] Y. Liu, J. Cai, N. Olgac, Q. Gao, A robust delayed resonator construction using amplifying mechanism, J. Vib. Acoust. 145 (1) (2023) 011010.
[27] B. Yan, X. Wang, Z. Wang, C. Wu, W. Zhang, Enhanced lever-type vibration isolator via electromagnetic shunt damping, Int. J. Mech. Sci. 218 (2022) 107070.
[28] B. Yan, Z. Wang, H. Ma, H. Bao, K. Wang, C. Wu, A novel lever-type vibration isolator with eddy current damping, J. Sound Vib. 494 (2021) 115862.

[29] N. Yu, K. Yang, Z. Wu, W. Zhang, B. Yan, Low-frequency vibration absorption of magnetic quasi-zero-stiffness structures with lever mechanism, Int. J. Mech. Sci. 267 (2024) 108973.
[30] Y. Shen, Z. Xing, S. Yang, J. Sun, Parameters optimization for a novel dynamic vibration absorber, Mech. Syst. Signal Process. 133 (2019) 106282.
[31] M. Baduidana, A. Kenfack-Jiotsa, Parameters optimization and performance evaluation for the novel tuned inertial damper, Eng. Struct. 250 (2022) 113396.
[32] M. Baduidana, A. Kenfack-Jiotsa, Analytical optimal design for the novel grounded three-element inertial damper, Eng. Struct. 272 (2022) 114964.
[33] T. Ikegame, K. Takagi, T. Inoue, Exact solutions to h∞ and h2 optimizations of passive resonant shunt circuit for electromagnetic or piezoelectric shunt damper, J. Vib. Acoust. 141 (3) (2019) 031015.
[34] H. Pu, Z. Sun, S. Yuan, X. Li, R. Bai, J. Yi, J. Zhao, J. Luo, Design, analysis and testing of an inerter-based passive sky-hook damper, Int. J. Mech. Sci. 260 (2023) 108633.
[35] K. Yamada, H. Matsuhisa, H. Utsuno, K. Sawada, Optimum tuning of series and parallel lr circuits for passive vibration suppression using piezoelectric elements, J. Sound Vib. 329 (24) (2010) 5036–5057.
[36] T. Asami, O. Nishihara, A.M. Baz, Analytical solutions to h∞ and h 2 optimization of dynamic vibration absorbers attached to damped linear systems, J. Vib. Acoust. 124 (2) (2002) 284–295.
[37] O. Nishihara, T. Asami, Closed-form solutions to the exact optimizations of dynamic vibration absorbers (minimizations of the maximum amplitude magnification factors), J. Vib. Acoust. 124 (4) (2002) 576–582.
[38] T. Asami, Optimal design of double-mass dynamic vibration absorbers arranged in series or in parallel, J. Vib. Acoust. 139 (1) (2017).
[39] T. Asami, Exact algebraic solution of an optimal double-mass dynamic vibration absorber attached to a damped primary system, J. Vib. Acoust. 141 (5) (2019).
[40] T. Asami, Y. Mizukawa, T. Ise, Optimal design of double-mass dynamic vibration absorbers minimizing the mobility transfer function, J. Vib. Acoust. 140 (6) (2018).
[41] T. Asami, O. Nishihara, Closed-form exact solution to h∞ optimization of dynamic vibration absorbers (application to different transfer functions and damping systems), J. Vib. Acoust. 125 (3) (2003) 398–405.
[42] O. Nishihara, Exact optimization of a three-element dynamic vibration absorber: minimization of the maximum amplitude magnification factor, J. Vib. Acoust. 141 (1) (2019).
[43] K. Yamada, T. Asami, Passive vibration suppression using 2-degree-of-freedom vibration absorber consisting of a beam and piezoelectric elements, J. Sound Vib. 532 (2022) 116997.
[44] H. Meng, X. Sun, J. Xu, F. Wang, The generalization of equal-peak method for delay-coupled nonlinear system, Phys. D: Nonlinear Phenom. 403 (2020) 132340.
[45] H. Meng, X. Sun, J. Xu, F. Wang, Establishment of the equal-peak principle for a multiple-dof nonlinear system with multiple time-delayed vibration absorbers, Nonlinear Dyn. 104 (2021) 241–266.
[46] G. Raze, G. Kerschen, H∞ optimization of multiple tuned mass dampers for multimodal vibration control, Comput. Struct. 248 (2021) 106485.
[47] X. Sun, J. Xu, F. Wang, L. Cheng, Design and experiment of nonlinear absorber for equal-peak and de-nonlinearity, J. Sound Vib. 449 (2019) 274–299.
[48] Y. Liu, J. Cai, L. Hou, B. Yan, L. Chen, Q. Gao, Bistable dynamics analysis using Padé approximation and resultant theory, Int. J. Non-Linear Mech. 149 (2023) 104325.
[49] Y. Liu, L. Cheng, Delayed resonator for complete vibration suppression of primary structures with nonlinear stiffness, Int. J. Non-Linear Mech. 161 (2024) 104689.
[50] Y. Liu, L. Cheng, A high-static-low-dynamic-stiffness delayed resonator vibration absorber, Commun. Nonlinear Sci. Numer. Simul. 140 (2025) 108299.
[51] J.J. Sylvester, XXIII. A method of determining by mere inspection the derivatives from two equations of any degree, Lond. Edinb. Dublin Philos. Mag. J. Sci. 16 (101) (1840) 132–135.
[52] Y. Liu, J. Cai, H. Li, Q. Gao, Optimal design and sensitivity analysis of the dynamic vibration absorber with amplifying mechanism, J. Comput. Inf. Sci. Eng. 23 (5) (2023) 051005.
[53] Q. Gao, J. Cai, P. Firoozy, S. Guo, H. Hong, Z. Long, Dixon resultant theory for stability analysis of distributed delay systems and enhancement of delay robustness, J. Franklin Inst. 359 (12) (2022) 6467–6485.
[54] J. Cai, Q. Gao, Y. Liu, A. Wu, Generalized Dixon resultant for strong delay-independent stability of linear systems with multiple delays, IEEE Trans. Autom. Control (2023).
[55] A.L. Dixon, The eliminant of three quantics in two independent variables, Proc. Lond. Math. Soc. 6 (4969) (1908) 209236.
[56] Q. Gao, N. Olgac, Bounds of imaginary spectra of lti systems in the domain of two of the multiple time delays, Automatica 72 (2016) 235–241.
[57] D. Kapur, T. Saxena, L. Yang, Algebraic and geometric reasoning using Dixon resultants, in: Proceedings of the international symposium on Symbolic and algebraic computation, pp. 99–107.
[58] I.M. Gelfand, M.M. Kapranov, A.V. Zelevinsky, A-Discriminants, Birkhäuser Boston, Boston, MA, 1994, pp. 271–296.
[59] A. Edelman, H. Murakami, Polynomial roots from companion matrix eigenvalues, Math. Comput. 64 (210) (1995) 763–776.
[60] G. Yan, Z.-Y. Wu, X.-S. Wei, S. Wang, H.-X. Zou, L.-C. Zhao, W.-H. Qi, W.-M. Zhang, Nonlinear compensation method for quasi-zero stiffness vibration isolation, J. Sound Vib. 523 (2022) 116743.